2010

Noise and multipath characteristics of power line communication channels

Hasan Basri Çelebi
University of South Florida

Noise and Multipath Characteristics of Power Line Communication Channels

by

Hasan Basri Çelebi

A thesis submitted in partial fulfillment
of the requirements for the degree of
Master of Science in Electrical Engineering
Department of Electrical Engineering
College of Engineering
University of South Florida

Major Professor: Hüseyin Arslan, Ph.D.
Chris Ferekides, Ph.D.
Paris Wiley, Ph.D.

Date of Approval:
Mar 30, 2010

Keywords: Power line communication, noise, cyclostationarity, multipath, impedance, attenuation

DEDICATION

This thesis is dedicated to my fiancée and my parents for their constant love and support.

ACKNOWLEDGEMENTS

First, I would like to thank my advisor Dr. Hüseyin Arslan for his guidance, encouragement, and continuous support throughout my M.Sc. studies. It has been a privilege to have the opportunity to do research as a member of Dr. Arslan's research group.

I wish to thank Dr. Chris Ferekides and Dr. Paris Wiley for serving in my committee and for offering their valuable feedback. I hope to be able to benefit from their profound knowledge and experience in the future, as well.

I owe much to my friends Sabih Güzelgöz, İbrahim Demirdöğen, Evren Terzi, Ali Görçin, Özgür Yürür, M. Bahadır Çelebi, Alphan Şahin, Murat Karabacak, M. Cenk Ertürk, Hazar Akı, Dr. Bilal Babayiğit, Dr. Mustafa Emin Şahin, Murad Khalid, İsmail Bütün, and Sadia Ahmed. We shared so many things with them. They also taught me so many virtues. Sincere friendship to start with, unselfishness, tolerance, and helpfulness. I am grateful to them for making me a better person.

I also would like to thank Tayyar Guzel and Dr. Murat Erat for helpful discussions and TUBITAK-UEKAE for providing the measurement equipment.

My sincere appreciation goes to my parents and my sisters Tuğba and Emine for always encouraging me for pursuing higher degrees. It is not possible to thank them enough, but I want them to know that I will be grateful to them throughout my life.

Last, but by no means least, my deepest gratitude goes to my fiancée, Rabia, for her love, all the sacrifices she made, her firm support, her vast patience, and her steady encouragement. I want to thank her from my heart for everything she has been doing.

TABLE OF CONTENTS

LIST OF TABLES

LIST OF FIGURES

NOISE AND MULTIPATH CHARACTERISTICS OF POWER LINE COMMUNICATION CHANNELS

Hasan Basri Çelebi

ABSTRACT

With the recent developments in technology, information and communication technologies (ICTs) are becoming more widespread and one of the basic building blocks of every humans life. The increasing demand in broadband communication calls for new technologies. Power line communication (PLC) is one of the potential candidates for next generation ICTs. Although communication through power lines has been investigated for a long time, PLC systems were never taken into account seriously because of its harsh communication medium. However, with the development of more robust data transmission schemes, communication over the power lines is becoming a strong alternative technology because of the existence of the infrastructure and the ubiquity of the network.

In order to establish reliable communication systems operating on power line networks (PLNs), characteristics of power line channels have to be investigated very carefully. Unpredictable characteristics of PLNs seriously affect the performance of communication systems. Similar to the other communication channels, PLC environment is affected by noise, attenuation, and multipath type of channel distortions. The level of noise in PLNs is much higher than any other type of communication networks. Furthermore, the frequency dependent attenuation characteristics of power lines and multipath stemming from impedance mismatches are the other distortion factors which have to be investigated in order to establish a reliable PLC system.

In this thesis, we focus on modeling of noise, frequency dependent attenuation, and multipath characteristics of power line channels within the frequency range between 30kHz and 30MHz.

CHAPTER 1

INTRODUCTION

In the late 1980's, it had been observed that, fixed telephone services used only a part of the frequency band available for communication in the copper cables. This idea led to the invention of digital subscriber line (DSL) technologies. By using this unused frequency bands, today, millions of houses throughout the world are getting broadband Internet access services via DSL. The emergence of communication over power lines is similar. Current standard alternating current (AC) electricity is being transmitted with frequencies at 50 or 60Hz, depending on the region of the world. Hence, it is not hard to see that, almost the entire frequency band is available for other additional applications. Consequently, it was proposed to transmit data over the unused frequencies of the power lines.

1.1 Advantages of PLC Systems

The concept of using the power lines for high speed data communication is not new. Communication over power line has been investigated since 1980's [1], however, it was never seriously taken into account because of harsh channel characteristics. For several years, power line communication (PLC) has been used for low data rate transmission with the data rates up to a few kilobits per second. However, recent trend in PLC requires the transformation of the electricity network into high data rate communication medium due to its inherent advantages. Advantages of PLC systems can be listed as follows:

- The existence of the infrastructure and the unrivalled ubiquity of the network, which virtually reaches anywhere in the world, makes the PLC medium very promising for many communication applications such as Internet, data and voice transmission.

- Due to the ubiquity of the existing infrastructure, low-cost broadband may become a reality in areas that cannot get DSL, cable or wireless broadband. Even homes in extremely remote areas could now potentially get broadband communication access by PLC systems instead of satellite broadband communications which suffer from high latency problem.

- PLC systems will allow broadband Internet access from every socket in every room which provides the availability to have the access to the Internet everywhere.

- Since the system does not need any additional installations, PLC systems are introduced as plug-and-play devices which are very cost effective and very easy to install.

- PLC systems are accepted as one of the most promising communication opportunities for smart home applications. It will provide the opportunity to remotely control the Internet-enabled household appliances without any additional installations. With this system, it will be possible to control your refrigerators, heating systems, smoke and fire alarm systems from the Internet. This idea will aid people with mobility problems.

1.2 PLC Systems

A simple PLC system is depicted in Fig. 1.1. The transmitter is located at the left and the receiver is on the right. The important parameters that effect the communication medium are the PLC channel itself, the noise added to the signal, and the impedance mismatches that occur along with the propagation of the signal.

In order to connect the PLC transceivers to the mains line, coupling circuits are used. These circuits are one of the must-have equipment for PLC systems. The coupling circuit placed between the transceiver and mains line to block the 50[1]Hz or 60Hz[2] frequency currents in order to protect the system from the mains line voltage.

[1]This mains line frequency with 50Hz and voltage with 230V has being used in Europe. The reason for that is at the beginning of twentieth century German AEG was the only power on electrical devices in Europe. AEG decided that 50Hz is more metric-friendly so they wanted it to be 50Hz [2].

[2]Mains line voltage is estimated as 120V in the United States (US). The reason for that can be explained as; the light bulb that Edison had discovered were using 110V direct current (DC). To maintain all the bulbs even after converting the mains line to AC, the best approximation for the light bulbs was 120V AC. At the

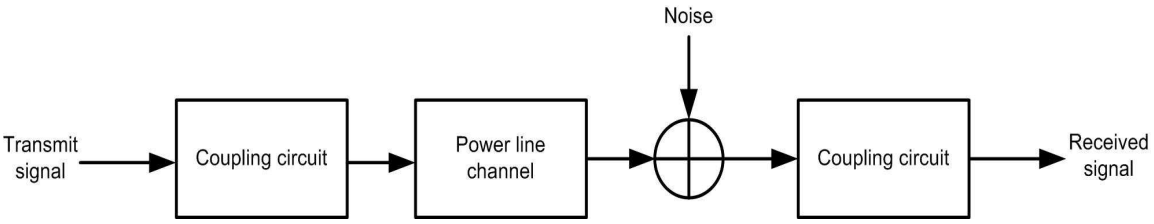

Figure 1.1 Graphical illustration of the PLC channel

PLC systems are also vibrantly marketing their importance, because in-expensive and easier-to-use systems. There are several indoor and outdoor applications for PLC systems. Indoor power line applications can be listed as follows [3–6]:

- Internet access for Internet protocol (IP) based devices,
- providing a home network for file sharing among computers, printers, cameras, televisions, speakers, gaming tools,
- data file transfer medium for home control systems such as remote monitoring, alarm systems,
- home automation systems for smart homes,
- in-vehicle network communication,
- remote detection of illegal electric usage,
- measuring the quality of power distributed to houses,
- communication tools for automated metering infrastructure (AMI) for smart grid systems,
    1. communication between electrical home devices and AMI for smart home applications,
    2. communication from house to the central access unit for smart grid systems.

same time, the mains line frequency was determined like the same way in Europe. Since the most prevalent company on electrical power systems was Westingtone at that time, the system that had been designed by them was implemented [2].

1.3 Standardization of PLC Systems

The only thing left for the PLC systems to penetrate the communication market is the availability of an international technical standard. Up to now, CENELEC and HomePlug standards are the most two popular standards for low data rate and high data rate PLC systems, respectively. CENELEC is a European organization and it was founded in 1973 as a non-profit organization under Belgian law. CENELEC standards are one of the very first published standards for PLC systems and it supports data rates up to 128kbps [7]. HomePlug Powerline Alliance is a non-profit organization founded in the United States (US) by Cogency, Conexant, Enikia, Intellon, Netgear, RadioShack Co., Sharp, Panasonic, Cisco systems, Motorola, Texas Instruments, Atheros, NEC electronics, Gigle networks, GE energy, and Broadcom, together with several other participants [8]. The first standard released by the HomePlug Powerline Alliance group was HomePlug 1.0. It was published in 2001 and supports data rates up to 14Mbps [9]. The next HomePlug standard was revealed in 2005 and named HomePlug AV [10]. The main purpose of this standard was providing data rates up to 150Mbps.

To regulate all the released standards throughout the world and publish an international technical standard for PLC systems, IEEE founded a new working group (WG) in 2005 namely IEEE P1901 WG [11]. This WG is a merge of Panasonic and HomePlug Powerline Alliance members. The scope of the P1901 WG is to develop an international standard for high-speed communication devices through AC electric power lines using frequencies below 100 MHz. The goal is to reach data rates up to 100Mbps [12].

1.4 PLC Channel

Although PLC systems are becoming popular because of its existing infrastructure. Since the main purpose of the power lines was not transmitting high frequency signals, therefore, power line network (PLN) offer extremely adverse environment for high frequency signals. Similar to any communication environment, attenuation, multipath stemming from

impedance mismatches, and noise are the three distortion factors which play an important role in the performance of communication systems over power lines.

- *Noise* in PLC channels is generated by all the electrical appliances connected to the grid and it is also caused by the coupling of the radio broadcasters which transmit their signals over short, middle, and long wave ranges.
- *Attenuation* is the loss of the power of the signal during its propagation and it depends on the physical length of the channel and the transmission frequency band.
- *Multipath* effect in the power line channel is caused by the impedance mismatches and is mostly dependent on both the physical characteristics and the physical topology of the channel.

These factors determine the quality of the channel. The quality is mostly a parameter of the noise level at the receiver and the attenuation of the electrical signal at different frequencies. The higher the noise level, the harder it is to detect the received signal. If the signal gets attenuated on its way to the receiver it could also make the decision harder because the signal gets more hidden by the noise, which is expressed as signal-to-noise ratio (SNR) level of the signal. SNR is a measure to quantify how much a signal has been corrupted by noise and calculated as

$$\mathrm{SNR}_{dB} = 10\log_{10}\Big(\frac{P_{signal}}{P_{noise}}\Big) \tag{1.1}$$

A ratio higher than 0dB indicates more signal power than noise power.

Multipath effect of the channel is the other disturbance while transmitting data over the channel. Multipath phenomenon can be explained as the transmitted signal reaching the receiving circuit by two or more paths with different delays.

1.5 Outline of Thesis

Each of these distortion factors must be investigated in detail in order to establish reliable PLC systems. It is worth mentioning that investigation of each of these channel

parameters requires exhaustive filed tests and measurements. Due to the amount of effort required for understanding their characteristics, the analysis will focus on only two of the above-mentioned factors. In this respect, noise and multipath in PLC systems will be the main focus of this thesis.

In Chapter 2, noise in PLC channels is investigated[3]. A simulation model for PLC channels is introduced in Chapter 3. Multipath and attenuation characteristics of PLC channels are analyzed in Chapter 4. In Chapter 5, effects of different PLN topologies on PLC channels are discussed.[4]. Conclusions and future studies are summarized in Chapter 6.

[3]This work is to partly appear in [13, 14]
[4]This work is to partly appear in [13, 15, 16]

CHAPTER 2

NOISE IN PLC CHANNELS

In conventional communication systems, noise is usually modeled as additive white Gaussian noise (AWGN). However, the measurements show that this model is not valid for PLC channel. Noise in PLC systems consists of colored background noise, narrow-band noise, and impulsive noise.

- *Colored background noise* results mainly from the summation of harmonics of mains cycle and different low power noise sources present in the system. Colored background noise is usually characterized with a power spectral density (PSD) decreasing with the frequency.

- *Narrow-band noise* is caused by ingress of amateur radio and radio broadcasters in long, middle, and short wave ranges. It mainly consists of sinusoidal signals with modulated amplitudes.

- *Impulsive noise* is generated mostly by electrical appliances plugged into the PLN. This type of noise is considered as the most significant among all type of noise sources in PLC. Impulsive noise is classified as:

  - *Periodic impulsive noise synchronous with the AC cycle* is caused by the rectifier diodes used in power supplies which operates synchronously with the mains cycle.
  - *Periodic impulsive noise asynchronous with the AC cycle* is generated by switched-mode power supplies and AC/DC power converters.
  - *Aperiodic impulsive noise* is caused by switching transients.

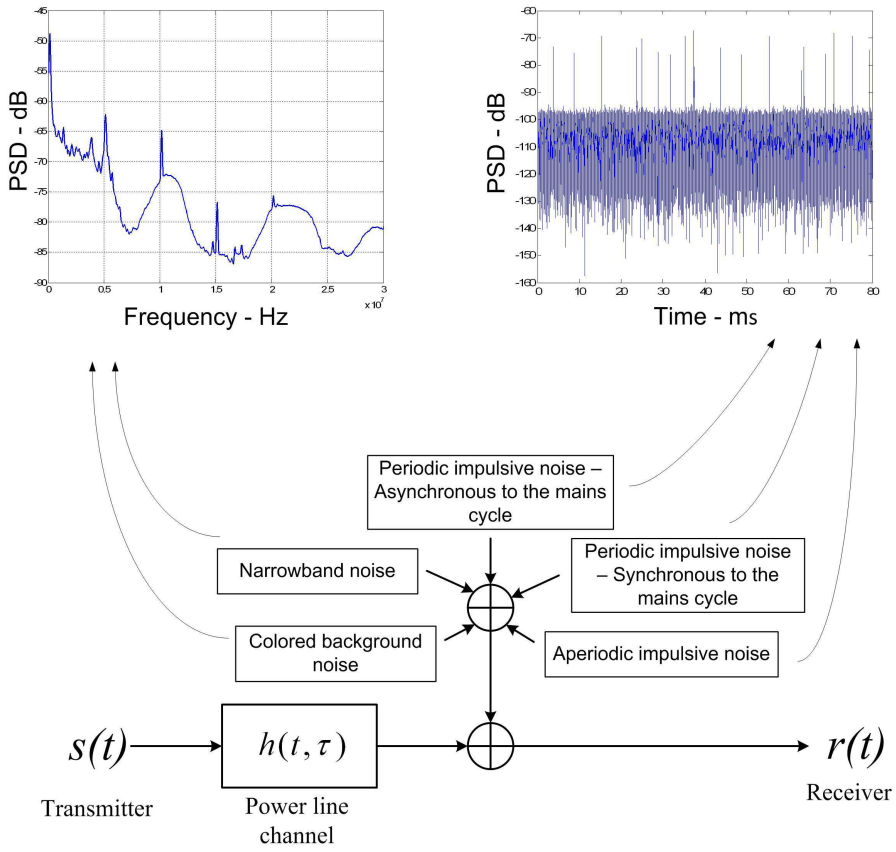

Figure 2.1 Noise types observed in PLC systems

The main sources of the impulsive noise are various electrical devices connected to the power line network. Impulsive noise needs to be characterized very carefully since it plays an important role in the performance and reliability of the PLC systems. Some studies investigating the impulsive noise characteristics of PLC channel are available in the literature. Noise characteristics of power line networks in various buildings are investigated in [17–20] by performing measurements at different power outlets. It is worth mentioning that understanding the impulsive noise characteristics of electrical devices individually is essential from the communication aspect. In this respect, some results on noise characteristics of different electrical appliances are presented in [21, 22] as well. In this study, a particular measurement setup is established in order to investigate the noise characteristics of various electrical devices. The measurement setup is designed in a way that it significantly reduces

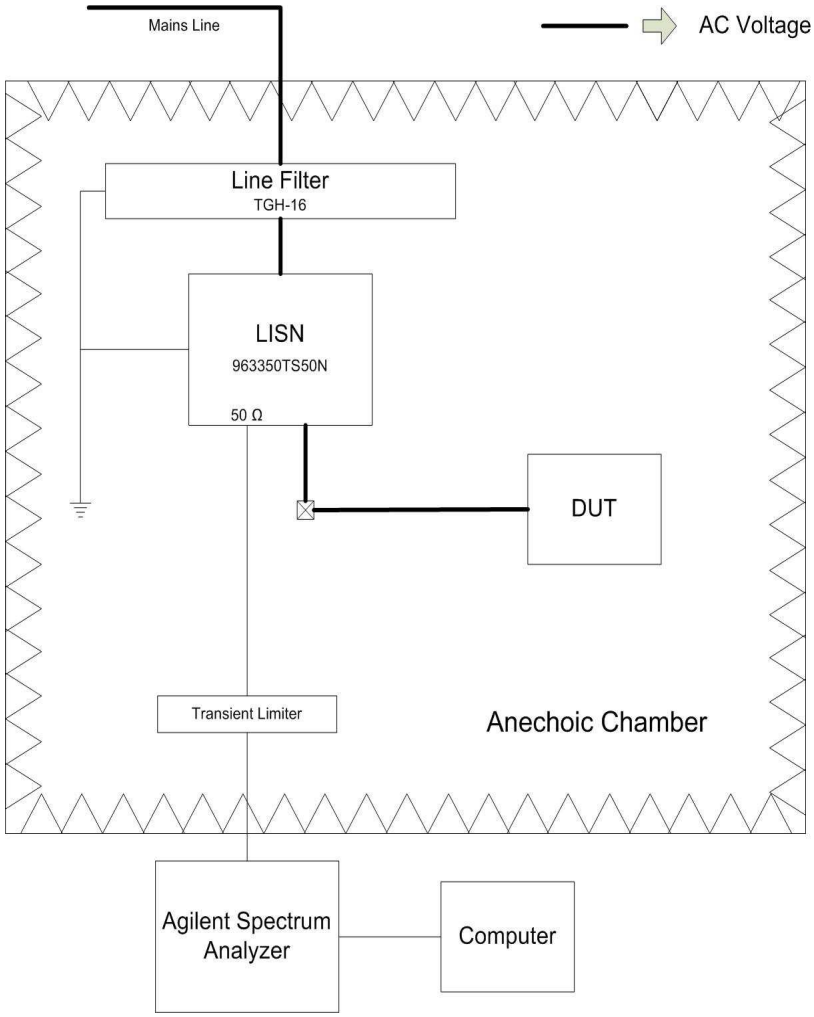

Figure 2.2 Pictorial description of the measurement setup

the noise power of other undesired noise sources such as narrow band noise and the noise generated by the other electrical loads within the power line network.

2.1 Measurement Setup

In order to investigate the impulsive noise characteristics of the electrical home devices, all other types of noise, namely colored background noise, narrow band noise, and impulses coming from PLN, have been suppressed by establishing an experimental environment which is depicted in Fig. 2.2.

List of the equipment that was used in the experiments is as follows:

1. anechoic chamber
2. power line filter
3. line impedance stabilization network (LISN)
4. transient limiter
5. Agilent E4440A PSA series spectrum analyzer

2.1.1 Anechoic Chamber

Anechoic chambers are shielded rooms fitted with Radio Frequency (RF) absorbers. The main goal of anechoic chambers is attenuating the electromagnetic signals to completely isolate inside the chamber from outside world activities. Since RF signals in low, middle, and long wave ranges are coupled to power line cables, in order to isolate both the device under test (DUT) and the cables inside the chamber from narrowband noise, anechoic chamber is used.

2.1.2 Power Line Filter

As described in the previous section, PLNs are affected from different noise sources. In order to increase the reliability of the measurements, rejecting all the noise coming from PLN is crucial. To suppress the undesired noise which may leak into the measurement setup from the mains line power line filter is used. The operating frequency of the power line filter ranges from 30kHz to 1GHz and provides more than 60dB attenuation between 100kHz and 1GHz [23].

2.1.3 LISN

In power line systems, the impedance of the network is not constant and changes with mains voltage. This fluctuation causes an impedance mismatch between measurement equipment and the line. This situation must be eliminated in order to enhance the ac-

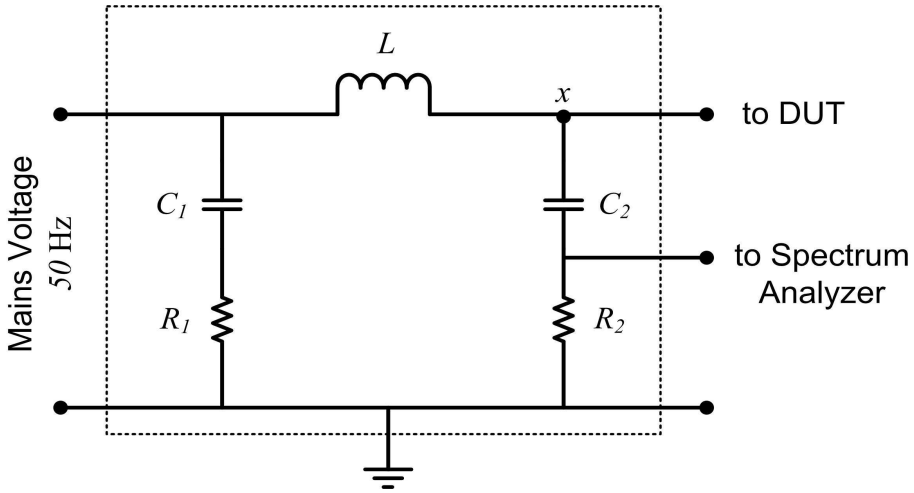

Figure 2.3 Block diagram of LISN

curacy of the measurement results. A line impedance stabilization network (LISN) is used for compensating this inconvenience and generating a known impedance value to get rid of impedance mismatches, which may hurt the reliability of the measurements. The second function of the LISN is isolating the measurement equipment from mains voltage.

Block diagram of LISN is depicted in Fig. 2.3. LISNs are "Pi-type" filters and they are very powerful electrical noise filters. A LISN mainly consists of two capacitors and one inductor as it is shown in Fig. 2.3. When the power comes from the mains line, capacitor C_1 offers very low reactance to high frequency components of the received noise and very high reactance to low frequency components. Consequently, noise at higher frequencies than 50Hz are rejected and only the low frequency components are kept. Since inductor L acts as a short circuit for low frequency components and open circuit for higher frequencies, all the components that belong to higher frequencies are filtered. As a result, only the low frequency components of the mains line will reach to DUT. When the DUT is turned on, the higher frequency components seen at point x will all belong to DUT and they will be prevented to go back to power line by the inductor L. Capacitor C_2 will act as the same as capacitor C_1 acts. It will transmit the higher frequency components of DUT while it blocks the components belong to lower frequencies such as the mains line voltage. As a result, with the help of the resistance R_2, higher frequency components of the noise, which

are generated by the DUT, will be captured by the spectrum analyzer in a very efficient and effective manner.

2.1.4 Transient Limiter

Transient limiter is integrated into the measurement setup to reject transients which may possibly damage the system hardware.

2.1.5 Spectrum Analyzer

Agilent E4440A PSA series spectrum analyzer was used in order to capture the noise characteristics of DUT. In every measurement, data with a duration of 200ms was recorded. Span of the spectrum analyzer is adjusted in a way that the frequency content of captured signal extends from 30kHz to 30MHz.

Throughout the measurement campaigns, all these measurement equipment itemized above as well as the DUTs except for the spectrum analyzer are placed inside the anechoic chamber. In addition, noise data is obtained by plugging each DUT individually into an outlet within the anechoic chamber not allowing any other device to share the same outlet at the time of the measurement.

In order to evaluate the effectiveness of the measurement setup before starting the experiments, noise level of two outlets, one inside and the other outside the anechoic chamber, are compared. As depicted in Fig. 2.4, a remarkable change is observed. It is clearly seen that the narrow band noise and the noise due to the electrical loads connected to the power line network are rejected successfully. For most of the frequencies, more than 20dB suppression of noise is achieved.

2.2 Noise Model and Measurement Data Processing

All the electrical devices connected to the PLN are becoming a noise source while they introduce different impedances to the network at termination points. It is possible to say for most of the electrical devices, due to the mains line, the noise generated and the impedance introduced by the devices are repeating itself for every cycle of AC voltage [24]. This makes

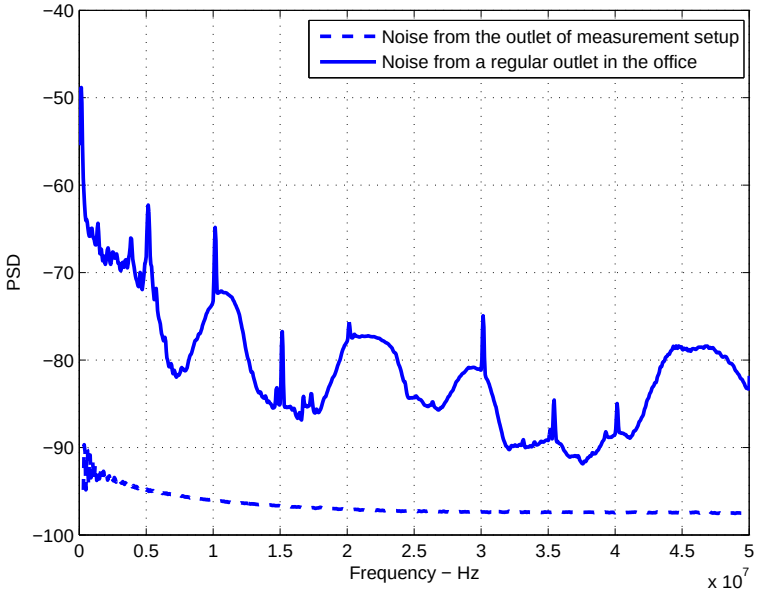

Figure 2.4 Noise levels of two outlets one inside and the other outside the anechoic chamber

the PLC medium a time variant channel. In this section, first the model of the noise in PLC systems that is widely employed in the literature will be given. Next, the measurement data processing which is based on the model provided will be detailed.

2.2.1 Noise Model

It is shown that, the instantaneous power spectral density (PSD) of the devices connected to the PLC network is found to be periodic with the mains voltage frequency [14]. This periodicity stems mainly from circuitry of the devices and can be 50Hz or 100Hz due to the fact that some of the devices are affected by the absolute value of the mains voltage, whereas some by its polarity. Due to their periodic structure, noise in PLC should be analyzed with a model whose parameters are related to the instantaneous value of the periodic mains line voltage. Consequently, cyclostationary random signal model is the best model to represent the noise generated by the electrical devices in PLNs.

A process, $n(t)$ is cyclostationary if its mean μ and autocorrelation functions denoted as $R(\cdot)$ satisfy the following conditions:

$$\mu(t + mT) = \mu(t) \tag{2.1}$$

$$R(t + \tau + mT, t + mT) = R(t + \tau, t) \tag{2.2}$$

The conditions set above indicate that the mean and correlation properties of the process do not change at the integer multiples of a period T. In PLC systems, T corresponds to half or one AC cycle period, T_0.

In order to verify the cyclostationarity of the noise and show that noise in PLC channels is repeating itself with a period of T or $T/2$, a simple analysis is performed on one of the devices measured by the measurement setup. The analysis is based on observing autocorrelation of the absolute value of the captured noise waveform over a duration that is a multiple of the AC cycle duration T_0. The result of the analysis, shown in Fig. 2.5, confirms the cyclostationary model. Note that the autocorrelation of the process is defined as follows:

$$R(t + \tau, t) = E\{n(t)n^*(t + \tau)\} \tag{2.3}$$

where $E\{\cdot\}$ is the statistical expectation operator, $(\cdot)^*$ denotes the complex conjugate of its input, τ is the time shift in the correlation operation.

Consequently, the instantaneous PSD of noise can be calculated by taking the forward fast Fourier transform (FFT) operation of the autocorrelation of the signal

$$S(t, f) = \int_{-\infty}^{\infty} R(t + \tau, t)e^{-j2\pi f\tau} d\tau \tag{2.4}$$

It can be seen that, the instantaneous PSD is time dependent and periodic as well. In order to eliminate the time dependency of (2.4) and reveal the average PSD of a cyclostationary process, an averaging over the duration of T_0 must be performed. The average PSD of a cyclostationary process is given by

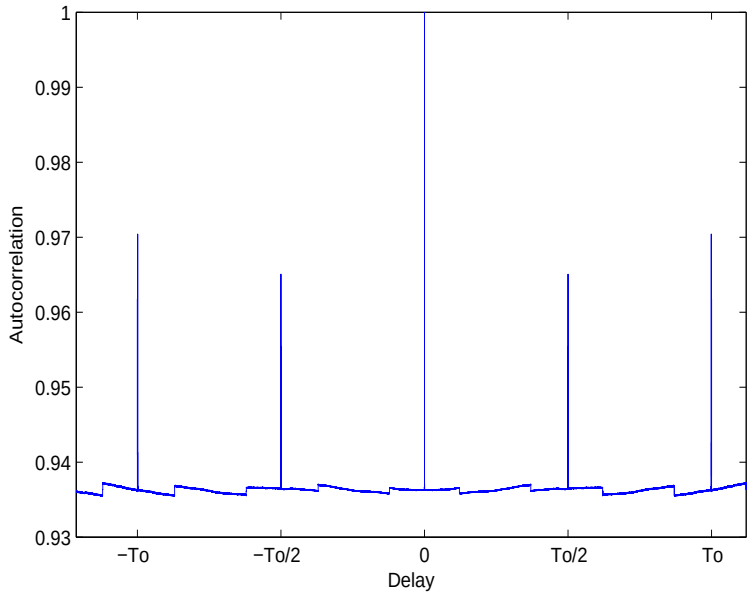

Figure 2.5 Autocorrelation of the absolute value of the noise generated by a light dimmer

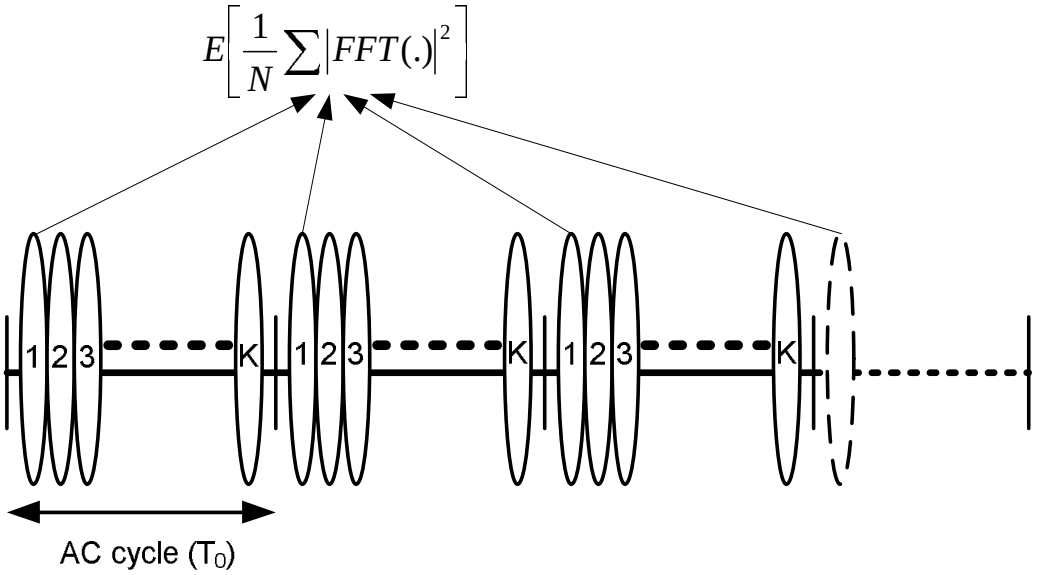

Figure 2.6 Processing of the captured data

$$S(f) = \frac{1}{T_0}\int_{-T_0/2}^{T_0/2} S(t,f)dt \tag{2.5}$$

2.2.2 Measurement Data Processing

It can be clearly seen from (2.4) that the periodicity in the autocorrelation function appears as a periodicity in the instantaneous PSD of the random process. Because of this inherent periodicity, time–frequency analysis (TFA) needs to be employed to reveal the cyclostationary feature of the noise generated by the devices. TFA is commonly used in the literature for characterizing and manipulating signals whose statistics vary in time. Since statistics of noise generated by devices are varying during one AC cycle, averaging the TFAs over several AC cycles is used to reveal the features of noise. In order to see the time evolution of the frequency content of the received noise, data denoted as n needs to be divided into sections considering the mains voltage period T_0.

Assume that the duration of the captured data equals the M multiple of T_0 and each section with the duration of T_0 is divided into K pieces. Note that the total duration of the recorded data equals MT_0. Let $N_{MK}(k,m)$ denote the discrete data samples falling into the kth piece within the mth AC cycle:

$$N_{KM}(k,m) = n(\frac{kT_0f_s}{K} + mT_0f_s : \frac{(k+1)T_0f_s}{K} + mT_0f_s) \tag{2.6}$$

where k and m are the factors that assume values from 0 to $K-1$ and from 0 to $M-1$, respectively. f_s is the sampling frequency of the measurement equipment that captures the noise data, $(x:y)$ implies the inclusion of discrete data samples from start position x till y. If the periodogram of (2.6) is averaged by considering each of the pieces falling into the same phase of the AC cycle, the following expression is obtained:

$$S_{N_{KM}}(k,m) = \frac{\sum_{m=0}^{K-1} \frac{K}{T_0f_s} |FFT(N_{MK}(k,m))|^2}{M} \tag{2.7}$$

where $FFT(\cdot)$ corresponds to forward FFT operation. Note that the time resolution of the TFA is equal to $\frac{T_0}{K} = T_r$. For the ease of understanding, this operation is illustrated in Fig. 2.6. As can be clearly seen, it basically averages the periodogram of each kth piece in every AC cycle.

Impulsive noise characteristics of various types of electrical home devices have been measured; however, only ten devices, which are considered to be the most significant noise sources, are investigated. These devices are as follows: computer tower, dimmer, drill, vacuum cleaner, TV set, LCD monitor, CRT monitor, fluorescent, laptop charger, and washing machine. Results are shown in the Fig. 2.9, Fig. 2.10. , Fig. 2.11, Fig. 2.12, Fig. 2.13, Fig. 2.14, Fig. 2.15, Fig. 2.16, Fig. 2.17, Fig. 2.18, and Fig. 2.19. In addition, in order to see the effectiveness of the measurement setup and the time variation of the background and narrowband noise in one AC cycle, TFA of noise captured from outside the chamber is depicted in Fig. 2.8.

Column *a* of the figures demonstrates the TFA of the noise generated by the electrical devices. The process while deriving this subfigure is formulated in (2.7) and illustrated in Fig. 2.6. Note that the power levels in TFA figures for each device are represented with different color codes. Column *b* is the demonstration of the time average of instantaneous PSD as defined in (2.5). A similar operation was performed along the frequency axis as well in order to see the noise power evolution over the duration of mains cycle. The outcome of this operation is plotted in column *c*.

Column *a*, *b*, and *c* show that each device exhibit unique characteristics from the perspective of both time and frequency. In order to quantify the concentration of the power over frequency, the bandwidth of the noise injected into the power line network is computed by considering the frequencies at which a 10dB decrease from the maximum power value is observed. In addition, if the noise floor is derived from Fig. 2.4, some important conclusions regarding the noise characteristics of the devices in frequency domain (column *b*) can be outlined as

- *Computer tower*: A noticeable rise is observed over the background noise as high as 55dB for the measurement frequency range with most of the power contained up to 4MHz

- *Dimmer*: A noticeable rise is observed over the background noise as high as 35dB for the measured frequency range with most of the power contained up to 5MHz

- *Drill*: A noticeable rise is observed over the background noise up to 45dB for the measured frequency range with most of the power contained between 11MHz–17.5MHz
- *Vacuum cleaner*: A noticeable rise is observed over the background noise up to 30dB for the measured frequency range with most of the power dispersed over various frequency ranges
- *TV set*: A noticeable rise is observed over the background noise up to 35dB for the measured frequency range with most of the power contained between 12.5MHz–21MHz
- *LCD monitor*: A noticeable rise is observed over the background noise up to 20dB for the measured frequency range with most of the power distributed over a broader range of frequencies with prominent spikes at some particular frequencies
- *CRT monitor*: A noticeable rise is observed over the background noise up to 20dB for the measured frequency range with power mostly distributed over a broader range of frequencies with prominent spikes around 4MHz, 10MHz, and 12.5MHz
- Fluorescent: A noticeable rise is observed over the background noise up to 10dB for the measured frequency range with most of the power concentrated around 5MHz
- *Laptop charger*: A noticeable rise is observed over the background noise as high as 15dB for the measured frequency range with most of the power contained up to 25MHz
- *Washing machine*: A noticeable rise is observed over the background noise up to 20dB for the measured frequency range with most of the power contained around 7MHz

Time domain characteristics (column c) of the devices are analyzed as well. The observations can be listed as

- *Computer tower*: Raise up to 45dB above the background noise floor for most of the AC cycle duration
- *Dimmer*: Raise up to 40dB above the background noise for a very short time over the AC cycle duration

- *Drill*: Raise up to 50dB above the background noise floor for a duration of $\approx$ 8ms
- *Vacuum cleaner*: Raise up to 20dB above the background noise floor covering half of the AC cycle duration
- *TV set*: Raise up to 30dB above the background noise floor for a duration of 4ms
- *LCD monitor*: Raise up to 13dB above the background noise floor covering most of the AC cycle duration
- *CRT monitor*: Raise up to 10dB above the background noise floor covering most of the AC cycle duration
- *Fluorescent*: Raise up to 6dB above the background noise floor covering half of the AC cycle duration
- *Laptop charger*: Raise up to 13dB above the background noise floor covering half of the AC cycle duration
- *Washing machine*: Raise up to 18dB above the background noise floor covering half of the AC cycle duration

In a similar procedure defined in [25], the cyclostationary behavior of the noise generated by electrical devices has been quantified by considering two parameters, namely peak excursion and maximum rate of change of the instantaneous PSD which are denoted as P_e and R_c, respectively. P_e indicates the maximum power change value during one AC cycle among all the frequencies, and R_c reveals the maximum power change in T_r second along the same frequency axis in one AC cycle. P_e and R_c are formulated as follows:

$$P_e = max\{10log_{10}[S_{N_{KM}}(t,f)]\} - min\{10log_{10}[S_{N_{KM}}(t,f)]\} \tag{2.8}$$

$$R_c = max\big\{\big|10log_{10}[S_{N_{KM}}(t+T_r,f)] - 10log_{10}[S_{N_{KM}}(t,f)]\big|\big\} \tag{2.9}$$

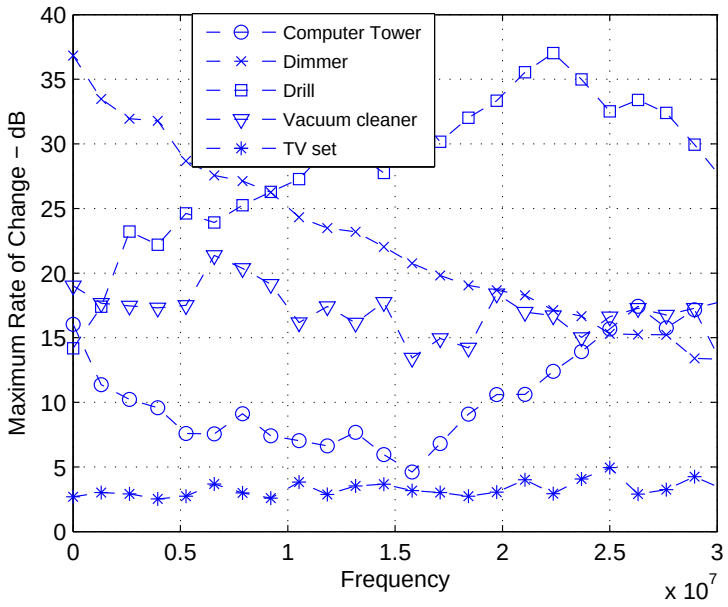

(a)

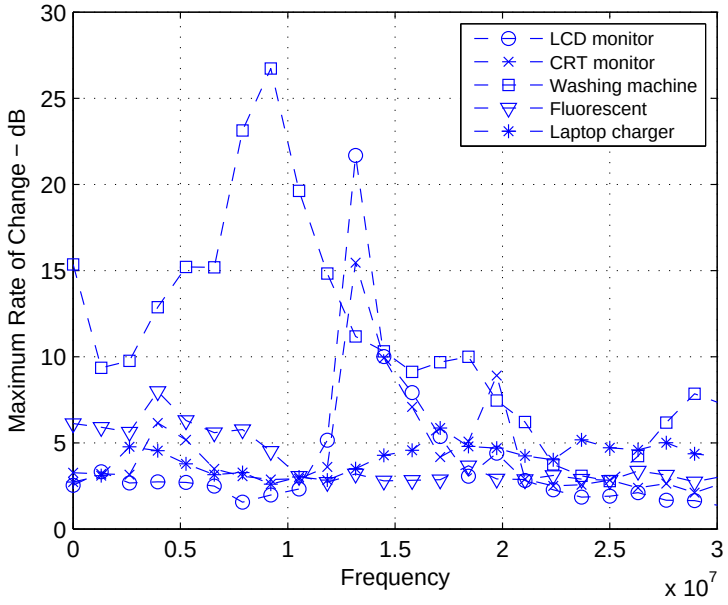

(b)

Figure 2.7 Maximum power of change for each frequency over an AC cycle

Results for the measured electrical devices are tabulated in Table 2.1. As can be clearly seen, computer tower and drill are the most significant noise sources.

Table 2.1 P_e and R_c of electrical loads

Measured device	P_e(dB)	R_c(dB)
Computer tower	61.26	17.43
Dimmer	45.61	36.83
Drill	59.66	37.03
Vacuum cleaner	42.49	21.92
TV set	42.13	4.95
LCD monitor	30.32	21.68
CRT monitor	28.75	15.45
Fluorescent	24.30	7.98
Laptop charger	23.47	21.12
Washing machine	40.81	26.72

In order to have a better understanding of the significance of devices, the maximum rate of change for each frequency has been plotted in Fig. 2.7(a) and 2.7(b).

Finally, in order to see the PLC noise when two or more devices are plugged into PLN at the same time, TV set and dimmer are placed together into the measurement setup and noise generated by devices is recorded and computed. the TFA analysis is shown in Fig. 2.20. TFAs of TV and dimmer noise are shown seperately in Fig. 2.14 and Fig. 2.11, respectively. As can be seen in Fig. 2.20, when these two devices are connected together, they still generate their noise independently from each other. Impulses generated by dimmer are located at 6.3ms and 16.3ms, while TV is continuously generating its noise, which proves the additive effect of noise in PLC.

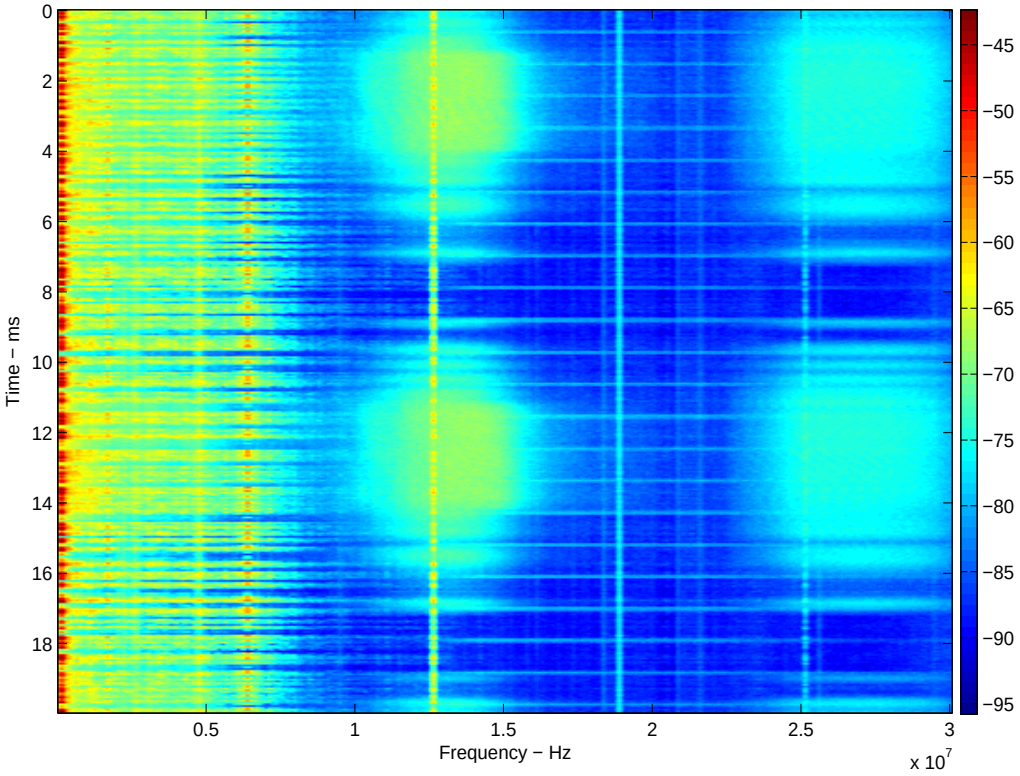

Figure 2.8 TFA of background noise captured from outside of the measurement setup

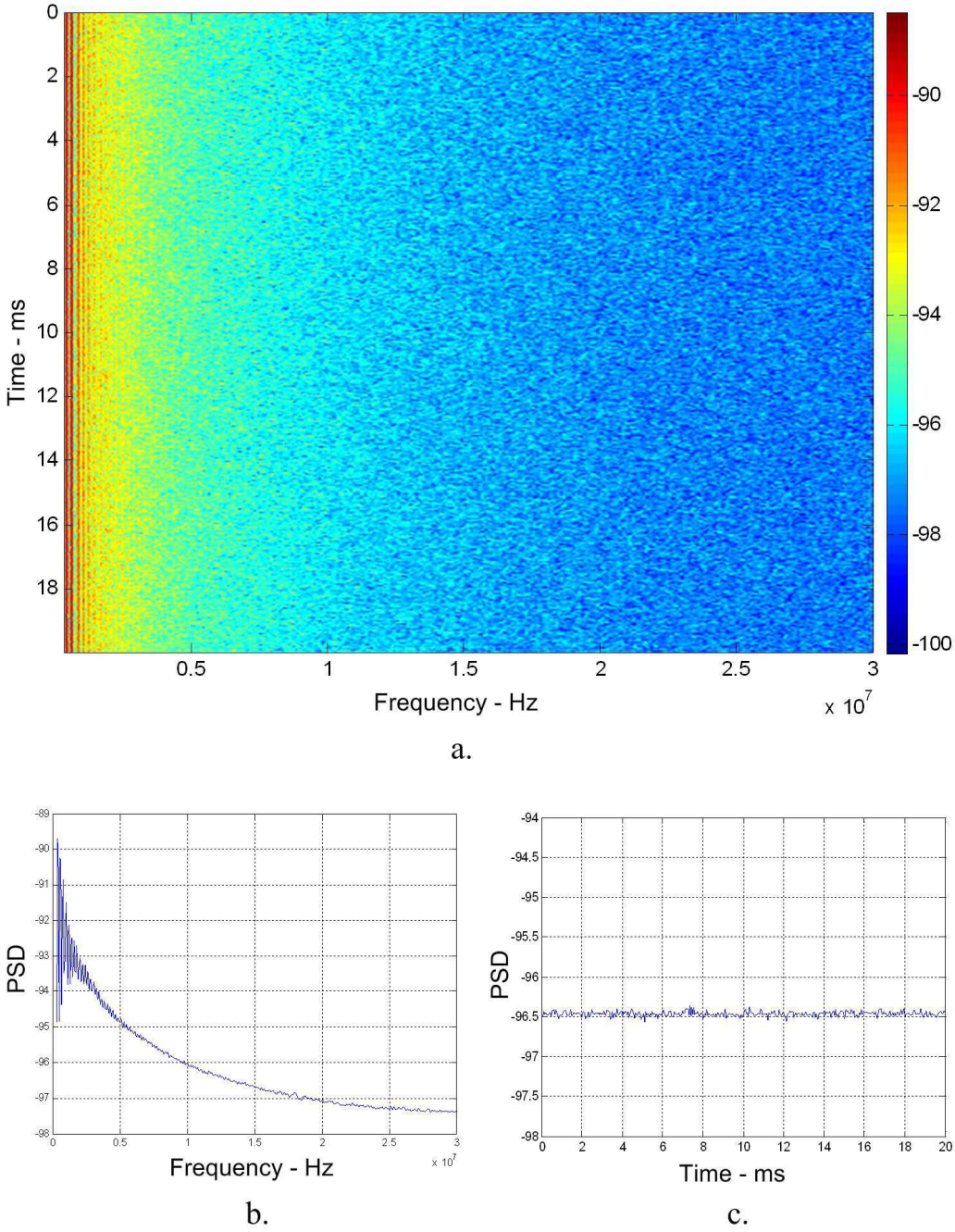

Figure 2.9 TFA of background noise in anechoic chamber

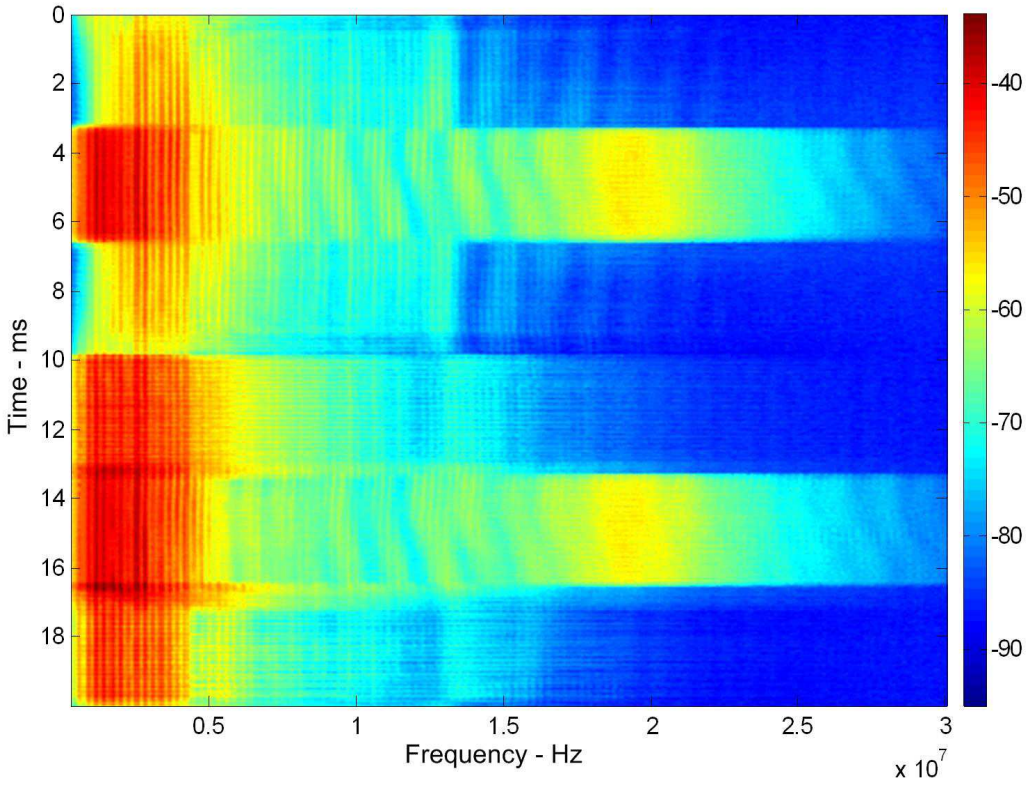

Figure 2.10 TFA of computer tower

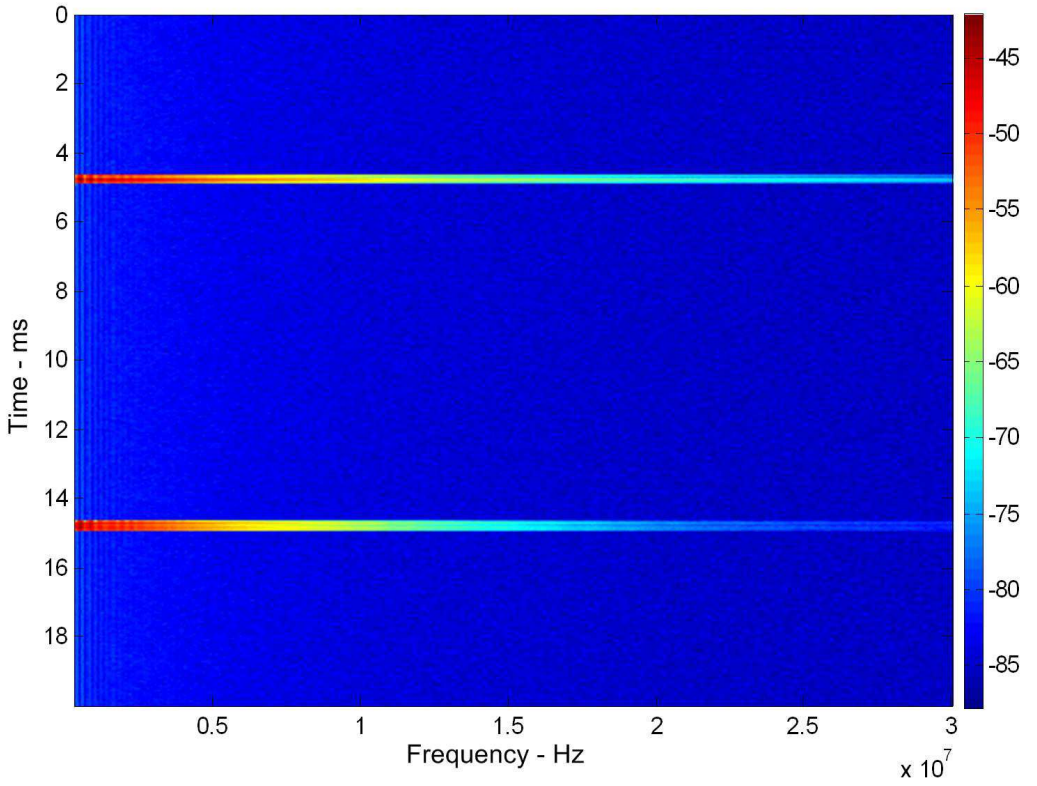

Figure 2.11 TFA of dimmer

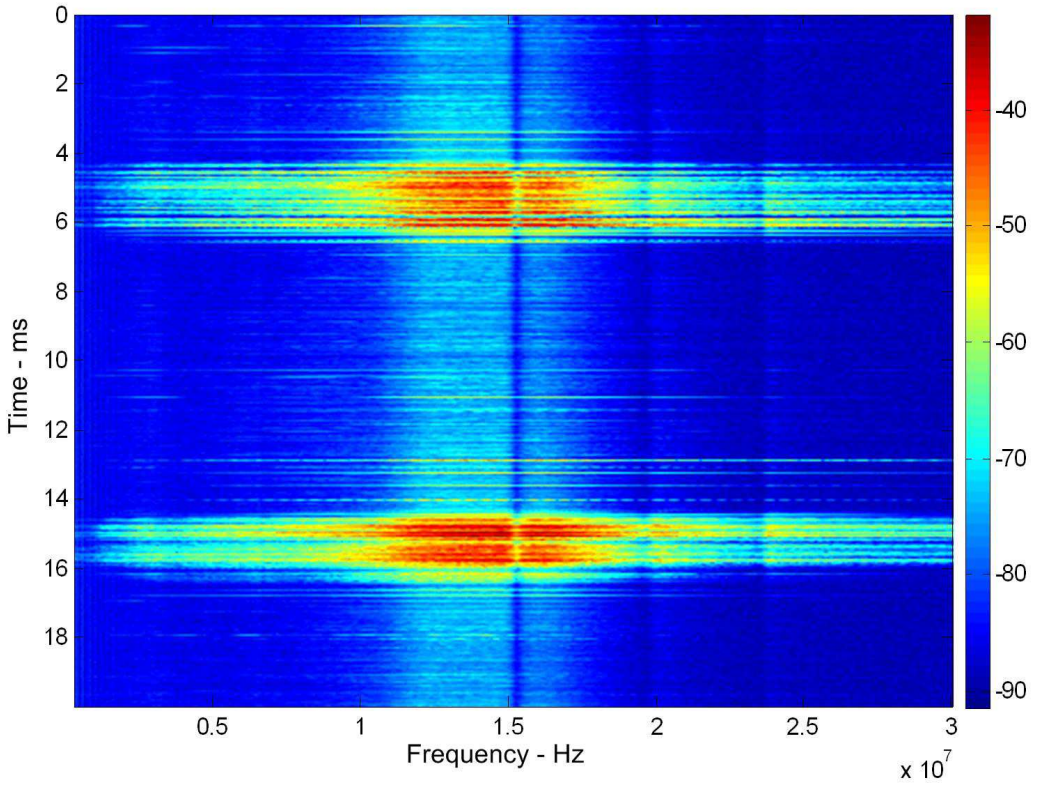

Figure 2.12 TFA of drill

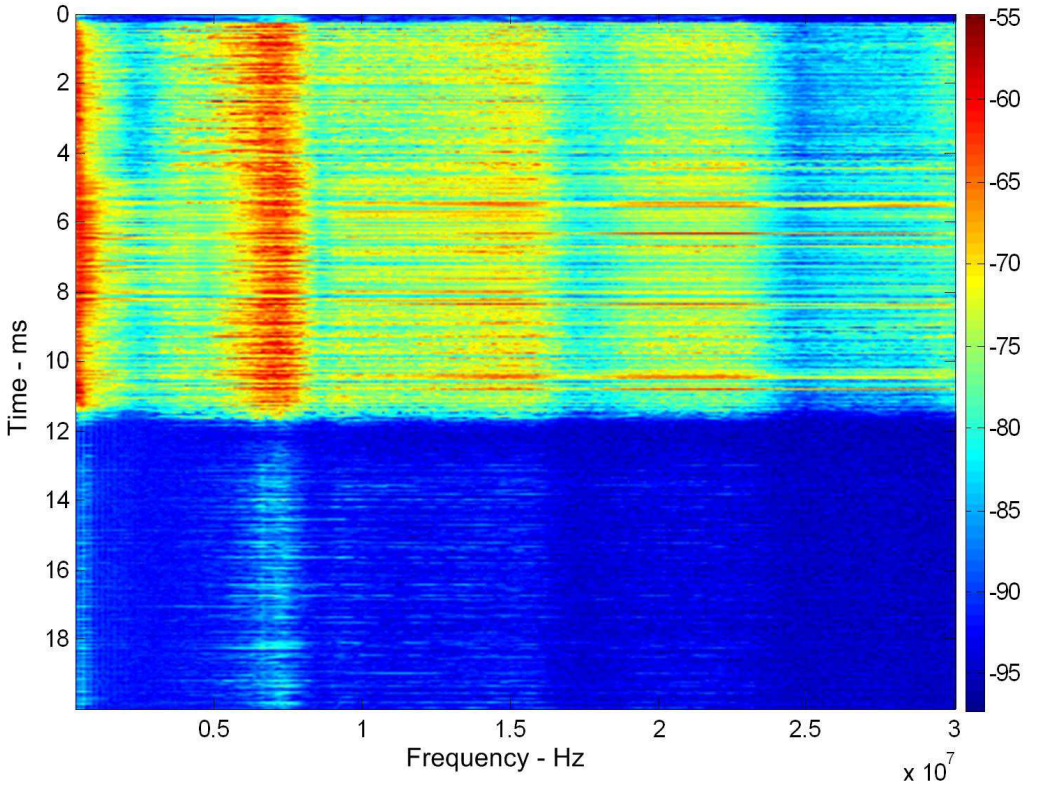

Figure 2.13 TFA of vacuum cleaner

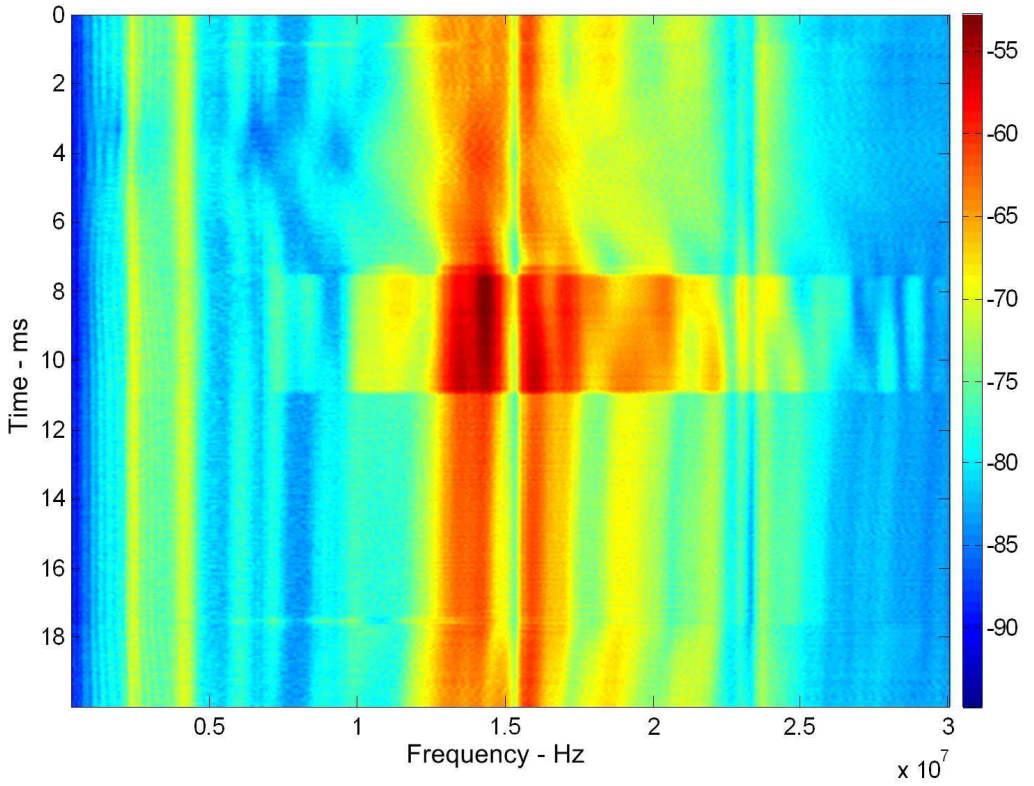

Figure 2.14 TFA of a TV set

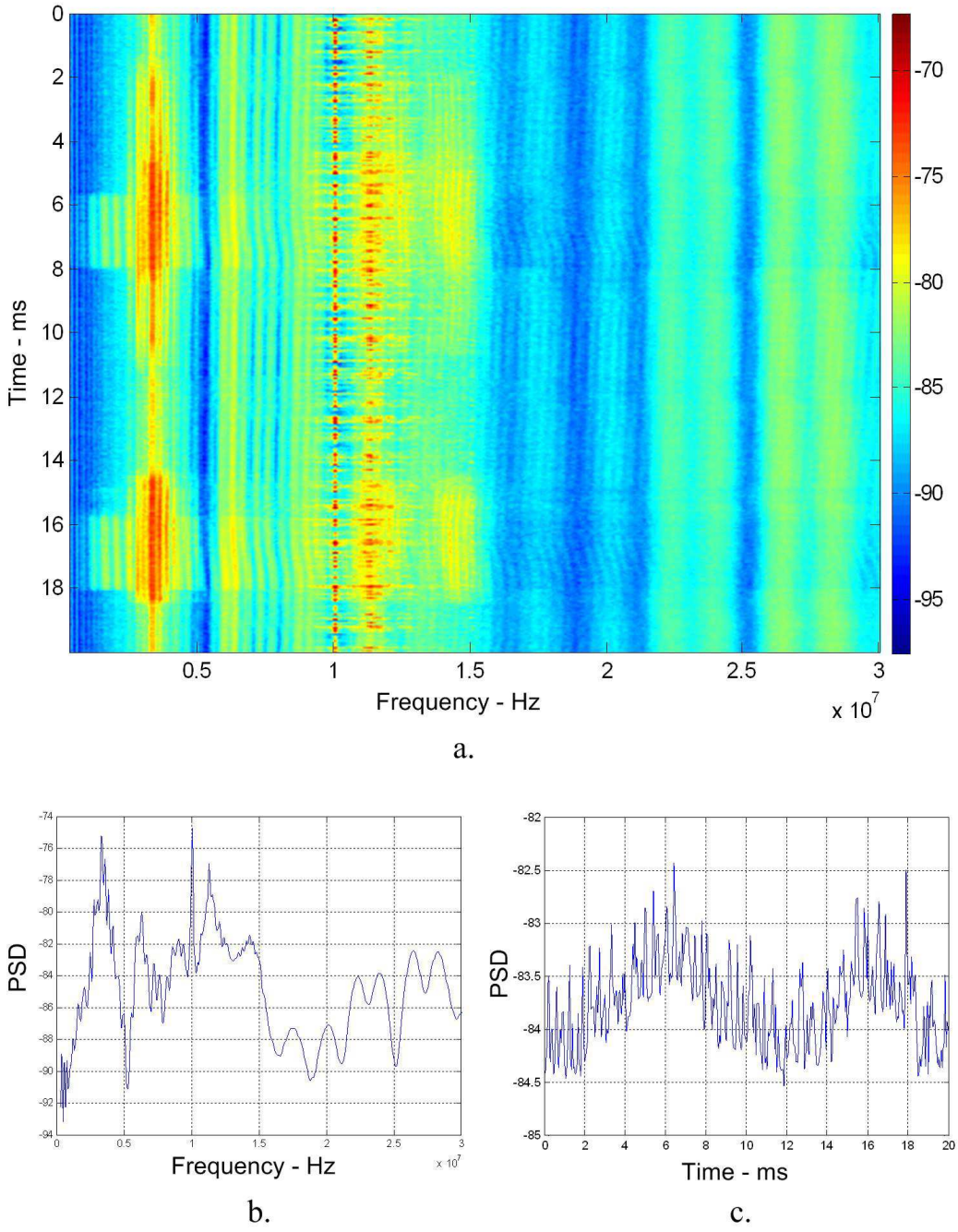

Figure 2.15 TFA of LCD monitor

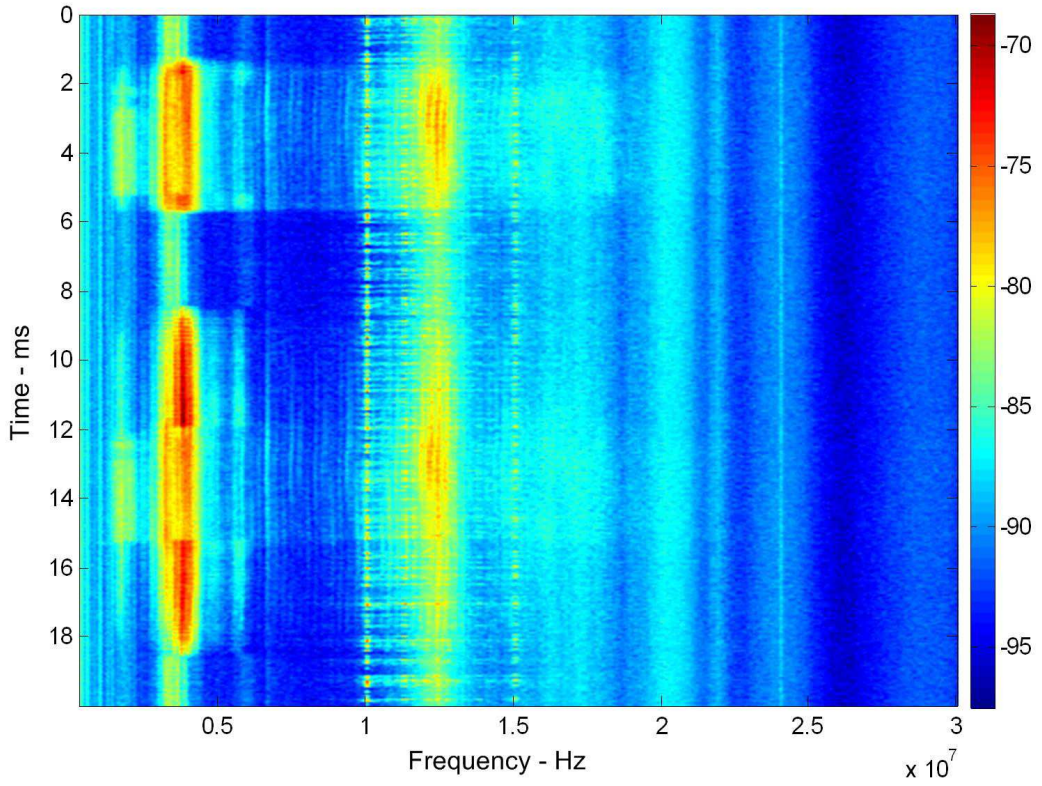

Figure 2.16 TFA of CRT monitor

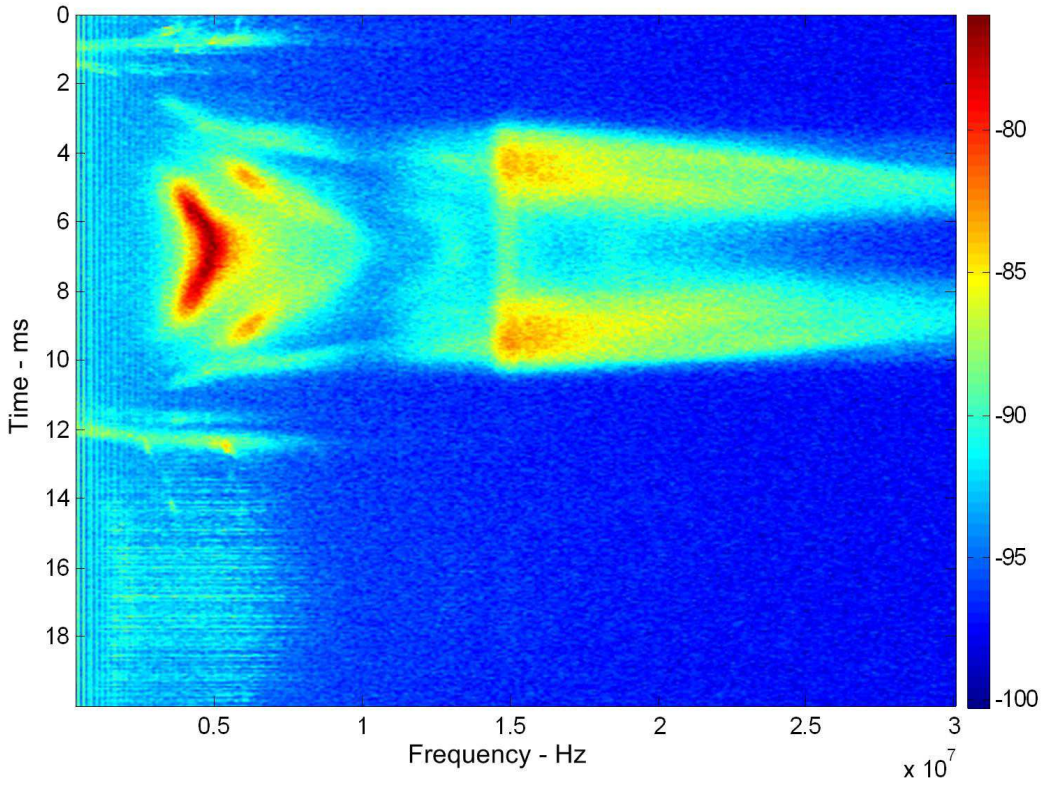

Figure 2.17 TFA of fluorescent

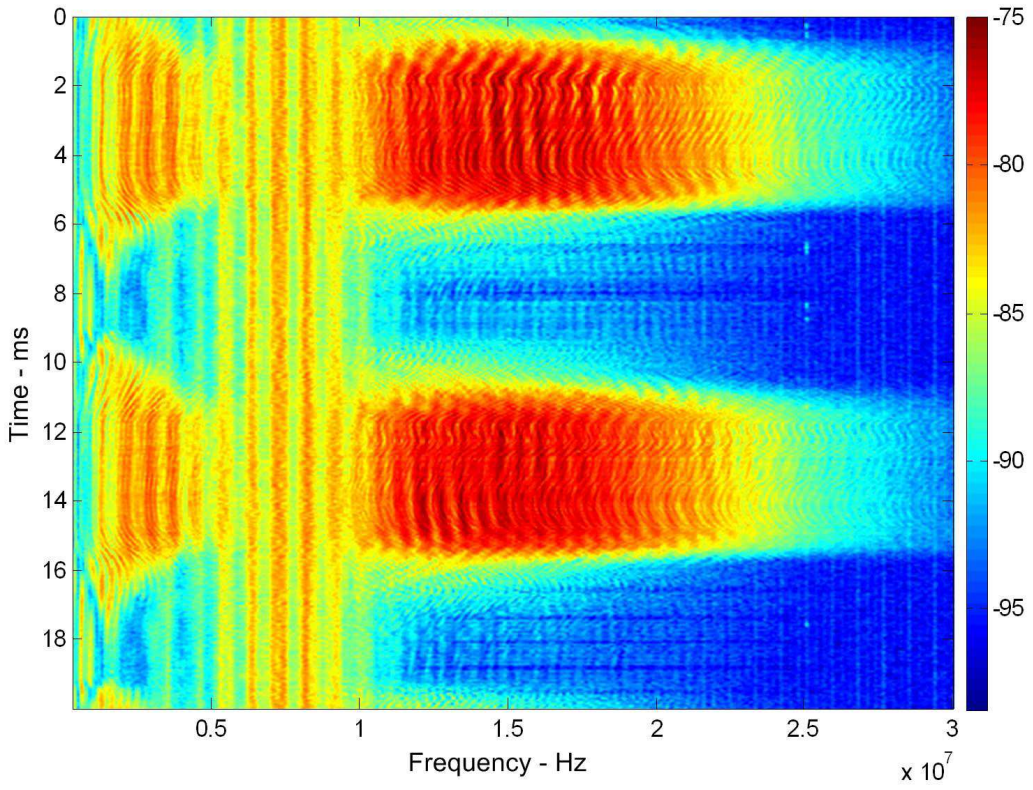

Figure 2.18 TFA of a laptop charger

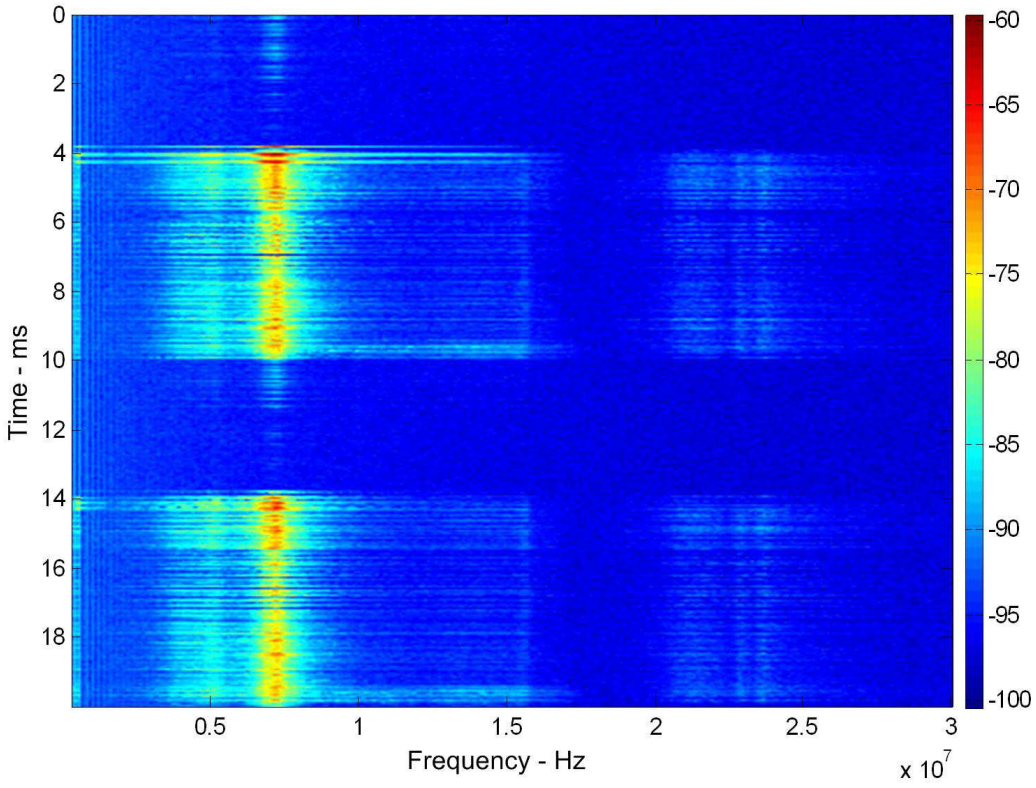

Figure 2.19 TFA of washing machine

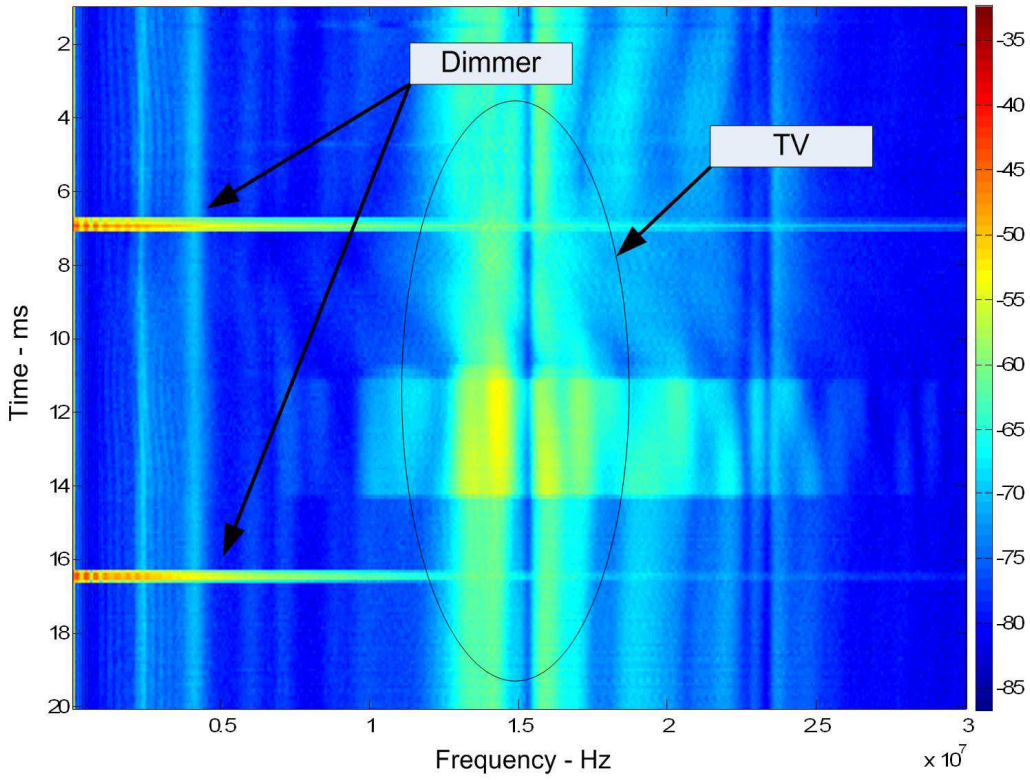

Figure 2.20 Additive effect of noise

CHAPTER 3

SIMULATING THE PLC NOISE

In this section, approaches proposed in the literature for simulating the noise in PLC channels will be discussed [17, 21, 26–29]. As it is mentioned in Sec. 2, noise in PLC systems can be classified in five categories, depicted in Fig. 3.1.

Background noise of PLC channels can be assumed as the addition of colored background noise and narrowband noise coupled to he power line cables [30]. The addition in frequency domain can be stated as

$$n_{bg}(f) = n_{cG}(f) + n_{nb}(f) \tag{3.1}$$

where $n_{bg}(f)$, $n_{cG}(f)$, and $n_{nb}(f)$ represent the total background noise, the colored background noise which is a colored Gaussian noise, and narrowband noise, respectively. The total background noise $n_{bg}(f)$ remains stationary for very long times, e.g. for several minutes or even hours [17, 31].

Among all the noise sources depicted in Fig. 3.1,

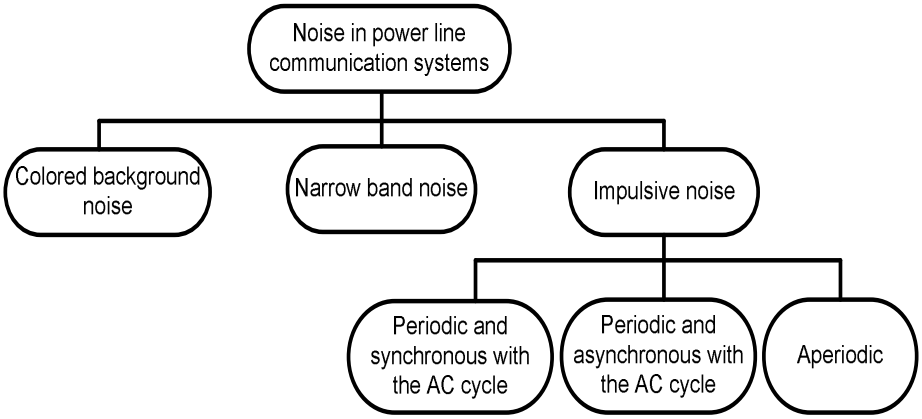

Figure 3.1 Noise types observed in PLC systems

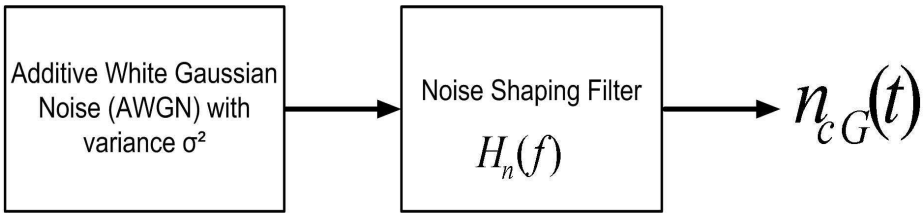

Figure 3.2 Generating the colored Gaussian background noise

- periodic impulsive noise - synchronous to the AC cycle,
- periodic impulsive noise - synchronous to the AC cycle, and
- aperiodic impulsive noise

are the most important noise sources in PLC channels, because their overall durations are in microseconds level which make them highly time varying and they cause most of the errors at data transmission [14, 28, 32].

Proposed power line noise takes all the noise sources under consideration and generates each noise type individually.

3.1 Background Noise

As stated before, PSD of background noise in PLC channels decreases with frequency. Its variation over time is very slow and accepted as to be stationary for long time of periods. Generation of the colored Gaussian background noise $n_{cG}(t)$ is depicted in Fig. 3.2.

The spectral shape of colored Gaussian background noise is obtained from the measurements. Since the scope of this measurement was to determine the colored Gaussian background noise of PLC channels, to reject the narrowband noise from PLN, anechoic chamber was used. The noise shaping filter $H_n(f)$ is depicted in Fig. 3.3.

3.2 Narrowband Noise

The second noise type that constitutes the total background noise is narrowband noise. Narrowband noise sources are mainly broadcast radio stations in short, middle, and long

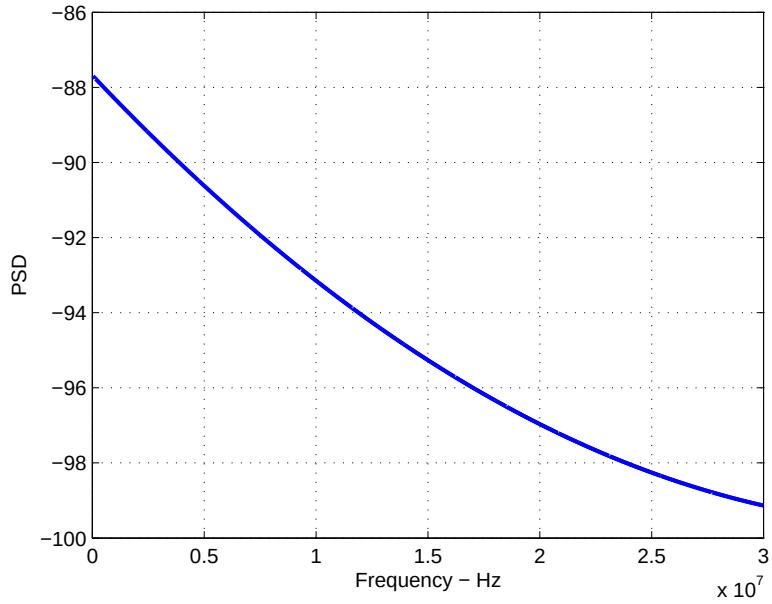

Figure 3.3 PSD of noise shaping filter

wave ranges. This type of noise consists of sinusoidal signals with modulated amplitudes [17] and can be described as

$$n_{nb}(t) = \sum_{k=1}^{N} A_k(t)\sin(2\pi f_k t + \varphi_k) \tag{3.2}$$

where N represents the total number of narrowband interferers, and $A_k(t)$, f_k, and φ_k describe the amplitude, central frequency and phase of the received narrrowband noise, respectively. Total number of interferers and their central frequencies can be extracted by empirical measurements and phase φ_k of each noise source can be selected randomly between $[0, 2\pi]$.

3.3 Impulsive Noise

The most significant noise sources in PLC channels that affect the quality of the transmission link are impulsive noise sources. Impulsive noise characteristics are studied in [29, 32] and their structures are discussed. It is found that, for most of the cases, structures of the impulses in PLC channels consist of damped sinusoids. As shown in the Sec. 2, the

most powerful contents of these impulses are located in low frequencies. The mathematical form of these impulses can be shown as sum of damped sinusoids with different frequencies

$$n_{imp}(t) = \sum_{k=1}^{N_D} A_k.\sin\big(2\pi f_k(t-t_p)+\varphi_k\big).e^{\big((-t-t_p)/\tau_k\big)}.\eta\Big(\frac{t-t_p}{t_\eta}\Big) \tag{3.3}$$

where N_D is the number of damped sinusoids that form the impulse, A_k represents the amplitude of the kth sinusoid, f_k denotes the pseudofrequency of the sinusoid, t_p is the arrival time of the impulses, φ_k represents the phase of the kth sinusoid, τ_k is the damping factor, and $\eta(t)$ denotes a square pulse with a duration of t_η. The amplitude value A_η of square pulse $\eta(t)$ is

$$A_\eta = \begin{cases} 1, & \text{if } 0 < t < t_\eta \\ 0, & \text{elsewhere} \end{cases} \tag{3.4}$$

The amplitude of each damped sinusoid A_k is selected to be $\sim \mathcal{N}(0, G_k\sigma_n^2)$ where G_k denotes the increment of the impulse over the background noise with a variance of σ_n^2. Values of G_k can change between $20-30$dB.

Throughout the simulations, impulsive noise types in PLC channels are analyzed into two categories

3.3.1 Periodic Impulsive Noise

It is found in [17] that most of the impulses received from PLC channels are periodic and has repetition rates between $50-100$Hz. Regarding to this result, the periodic arrival time of impulses t_p should be 10ms or 20ms. The overall duration time of impulses is measured around $50\mu s$ which is set to be the duration of the square pulse t_η. From the measurement results discussed in [29, 32], number of damped sinusoids N_D is determined as 3 and pseudofrequencies of the damped sinusoids are set as 300KHz, 2MHz, and 3.5MHz.

3.3.2 Aperiodic Impulsive Noise

The main difference between aperiodic and periodic impulses are their arrival times. In the simulations t_p values of these impulses are modeled as random variables. However, as discovered and explained in [31], distribution of interarrival time between two successive aperiodic impulses is modeled with an exponential distribution with mean of 100ms. Interarrival time of impulses can be formulated as

$$t_{int} = t_p(n) - t_p(n-1) \tag{3.5}$$

where $t_p(n)$ represents the arrival time of nth aperiodic impulse. The total duration of aperiodic impulses are set to $100\mu s$ and their amplitude variation are adjusted to be distributed as Gaussian like the periodic impulses.

Real and imaginary parts of a simulated impulse with a time duration of $50\mu s$ are depicted in Fig.3.4 and Fig.3.5, respectively. Finally, by using the simulation environment a realistic noise data for PLC channels is generated and plotted in Fig.3.6. Length of the generated noise is estimated as 80ms which is four AC cycles.

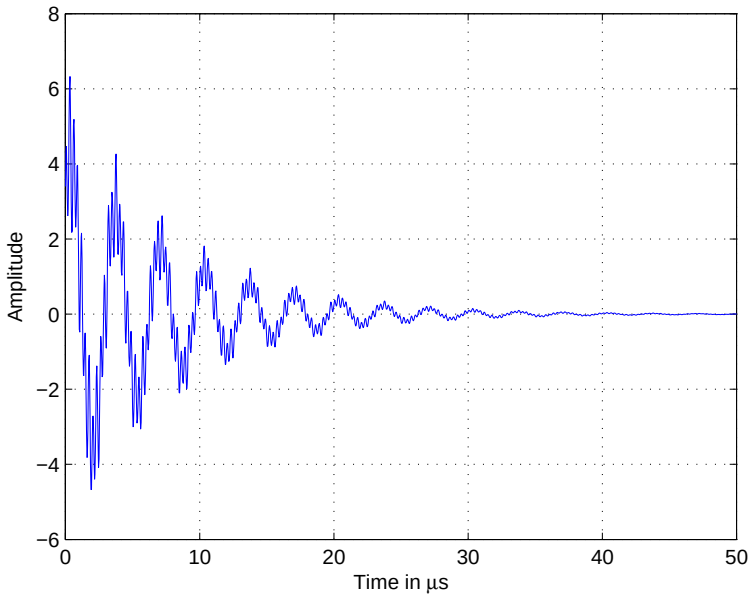

Figure 3.4 Realization of real part of an impulse noise

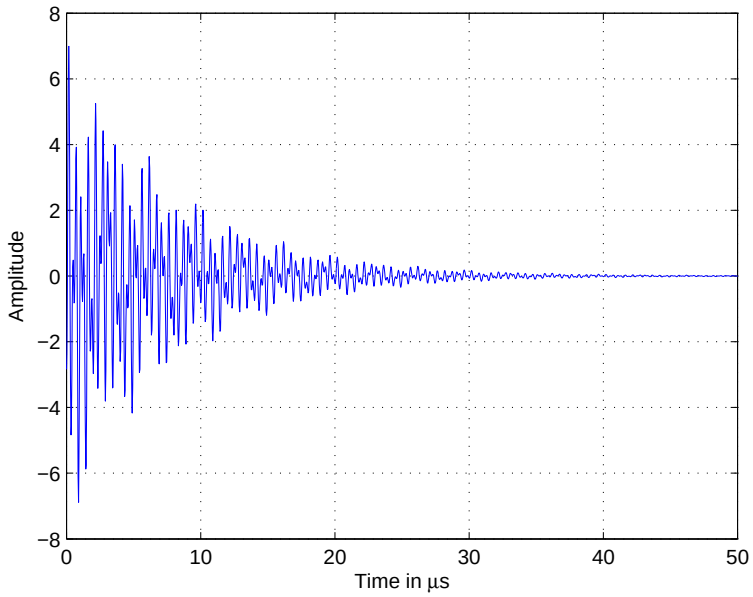

Figure 3.5 Realization of imaginary part of an impulse noise

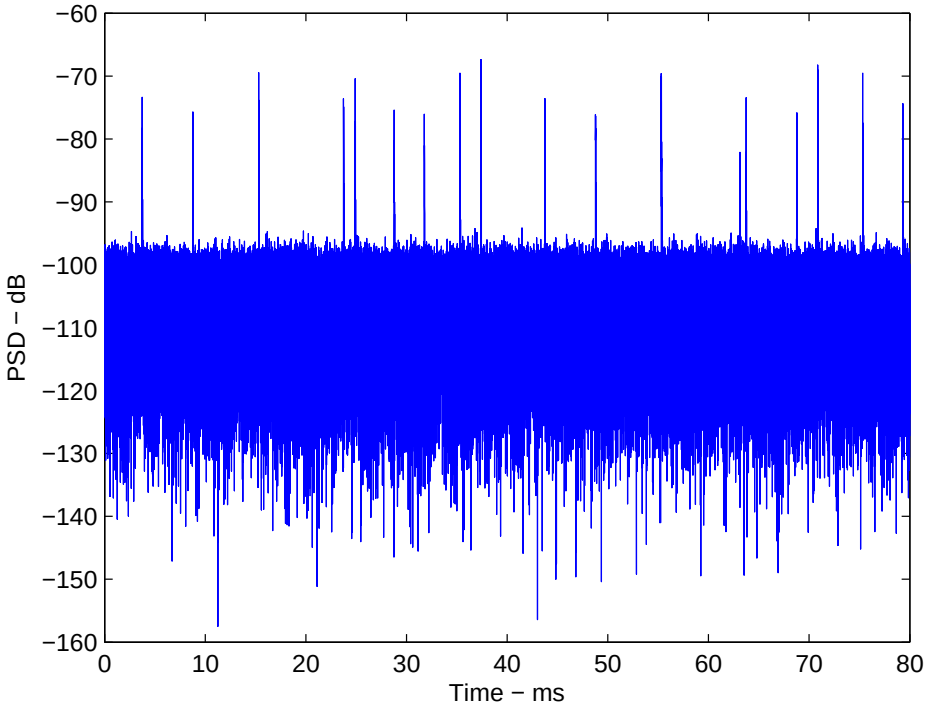

Figure 3.6 Simulated PLC noise

CHAPTER 4

MULTIPATH EFFECT IN PLC CHANNELS

Power lines are also affected from multipath phenomenon like wireless communication channels. In order to model the PLNs for high speed data transmission, multipath characterization of the PLNs has to be analyzed very carefully. Instead of point-to-point connections between transmitter and receiver, PLN topology follows a random bus topology type of distribution. For this reason, multipath phenomenon is becoming a very significant drawback in PLCs.

However, unlike the wireless communication mediums, since the topology of an indoor PLN is stable and immovable, analytical calculation of the frequency response of any point-to-point channel is possible by analyzing the multipath components of any specific indoor PLN. It is worth mentioning that, multipath components are mostly affected by the physical topology of the network, length of the cables, characteristic impedances of the cables and loads plugged into the termination points of the PLN. In order to come up with a realistic solution, priori knowledge about the PLN is needed.

In this section, first, multipath characteristics of PLC channels is given. Next, attenuation model, which is a significant factor while calculating the transfer function of a PLC channel, is derived. Measurement results are compared with the simulation results.

4.1 Multipath Phenomenon in Power-Line Channel

In power-line channels, signal propagation does not only take place through the closest path between transmitter and receiver. Reflections are caused because of the impedance mismatches in branching points and different loads plugged into the PLN. Characteristics of these reflections depend highly on the topology of the PLN and the electrical loads present

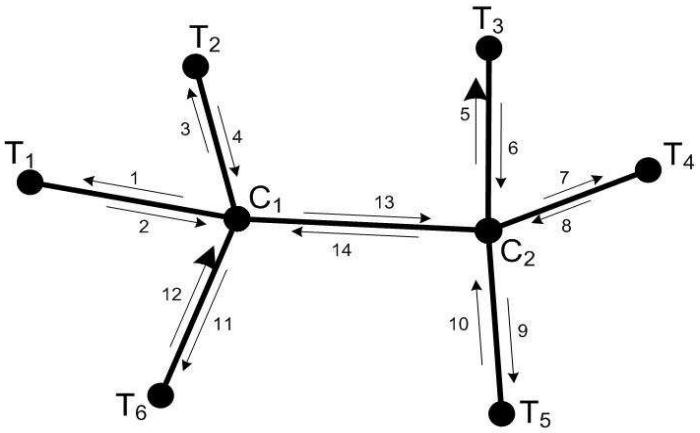

Figure 4.1 Example of an indoor PLN with the directional segments shown and numbered.

in the network. Even for a homogeneous network, where one type of cable is used, lots of reflections occur at branching points of cables and termination points where electrical loads are connected.

Example of a simple indoor PLN is depicted in Fig. 4.1. The possible signal propagation segments are shown and numbered. As can be seen from the figure, every line connected to the power grid causes two more directional paths which are opposite directions. So, the number of possible segments of a PLN is twice the total number of lines. In Fig. 4.1, the network consists of 8 nodes, 7 lines, and 14 possible directional segments. For instance, if the transmitter is located at the termination point named as T_2 and the receiver is located at T_5, various propagation paths can be defined by using numbered directional segments such as

$$4 \rightarrow 13 \rightarrow 9 \quad (\text{which is assumed as the line} - \text{of} - \text{sight (LOS) path})$$

$$4 \rightarrow 13 \rightarrow 14 \rightarrow 13 \rightarrow 9$$

$$4 \rightarrow 3 \rightarrow 4 \rightarrow 13 \rightarrow 9$$

$$4 \rightarrow 11 \rightarrow 12 \rightarrow 13 \rightarrow 9$$

$$4 \rightarrow 1 \rightarrow 2 \rightarrow 13 \rightarrow 7 \rightarrow 8 \rightarrow 9$$

$$\vdots$$

Theoretically, even in a very simple PLN, it is possible to define infinite number of different propagation paths. However, due to the frequency dependent cable loss in PLC channels and the transmission and reflection coefficients, which will be explained in the next section, power of the multipath components, which travel more, will decrease more than others. It can be generalized as, if the propagating length of a multipath component increases, it will affect more from the frequency dependent path-loss and more transmission and reflection coefficients will occur along its propagation path. Consequently, number of multipath components can be limited to a finite number of significant paths.

4.2 Transmission over Power-Line Channel

In PLC channels, when a signal propagates from one location to another, reflections occur at every impedance discontinuities along the propagation path. Main reasons of impedance mismatches can be defined as; different characteristic impedances of different cables, electrical devices plugged into the PLN from the termination points, and branching points where more than two cables are connected.

4.2.1 Reflection and Transmission Coefficients

The amplitude and phase ratio of reflected and transmitted energy to the incident signal is expressed by reflection coefficient and transmission coefficient, respectively. These coefficients are dependent to the characteristics impedance of cable and input impedances of loads.

Characteristic impedance of a cable is dependent to the cable's circuit coefficients and operating frequency, however, it has nothing to do with the length of the cable. Z_0 can be calculated as

$$Z_0 = \sqrt{\frac{R + jwL}{G + jwC}} \tag{4.1}$$

where Z_0 represents the characteristic impedance of the line the signal propagates, w is the angular frequency, and R, L, G, and C represent the per-unit-length resistance, inductance, conductance, and capacitance values, respectively. As it is shown in [33, 34], for the

frequency range planning to be used in PLC channels, equations result in $R << wL$ and $G << wC$. The simplified expression of Z_0 can be shown as

$$Z_0 \cong \sqrt{\frac{L}{C}} \tag{4.2}$$

Consequently, for the cables that are commonly used in power lines, characteristics impedance Z_0 and the impedance values of the loads connected to the termination nodes Z_L are assumed as real valued and independent from the operating frequency [33].

$$Z_0(f) = Z_0 \quad \text{and} \quad Z_L(f) = Z_L \qquad \text{for} \quad 30\text{kHz} \leq f \leq 30\text{MHz} \tag{4.3}$$

Since reflection and transmission coefficients are related to the impedance values, they are becoming frequency-independent too.

$$\Gamma(f) = \Gamma \quad \text{and} \quad T(f) = T \qquad \text{for} \quad 30\text{kHz} \leq f \leq 30\text{MHz} \tag{4.4}$$

where Γ and T denote the reflection coefficient and transmission coefficient, respectively. These two coefficients at a particular impedance discontinuity are given by the following equations (see Appendix A) [35]:

$$\Gamma = \frac{Z_L - Z_0}{Z_L + Z_0} \quad \text{and} \quad T = 1 + \Gamma = \frac{2Z_L}{Z_L + Z_0} \tag{4.5}$$

where Z_L is the impedance that the signal sees at the discontinuity.

A different way to calculate characteristic impedance of a cable is by measuring the input impedances of the cable with short and open-circuit termination endings [36]. The square-root of the product of these two input impedances gives the characteristic impedance

$$Z_0 = \sqrt{Z_{sc} Z_{oc}} \tag{4.6}$$

where Z_{sc} and Z_{oc} represent input impedance values of the cable with short and open-circuit endings, respectively.

4.2.2 Reflection Factor

The effect of numerous reflections and transmissions along the i^{th} propagation path is represented as the reflection factor which is formulated as the multiplication of all the reflection and transmission coefficients the signal sees. It quantifies the amount of total loss on the propagating signal stemming from the impedance mismatches present in the PLN. Reflection factor, denoted as $r_i e^{j\theta_i}$, is usually but not necessarily a complex number. Reflection factor of i^{th} path can be expressed as;

$$r_i e^{j\theta_i} = \prod_{k=1}^{K} \{\Gamma_{ik}\} \prod_{m=1}^{M} \{T_{im}\} \tag{4.7}$$

where K and M are the total reflections and transmissions seen by the transmit signal along a the particular propagation path, respectively.

However, since each received replica of the transmitted signal travels different length of paths, denoted as d_i, time delays occur among them and it shifts the phase of the signal. This factor depends on the length of the propagation path and the velocity of the propagation within the power line. The delay of the i^{th} path can be represented as;

$$\tau_i = \frac{d_i}{v} \quad \text{where} \quad v = \frac{c_0}{\sqrt{\varepsilon_r}} \tag{4.8}$$

where v represents the propagating velocity within the cable which depends on the speed of light c_0 and the relative dielectric constant ε_r of the insulating materials of the cable. Note that the speed of the propagation within the power line is assumed to be 60% of the speed of light in this study [37].

4.2.3 T Network Structure

In order to understand multipath phenomenon in a PLN, a T network structure, as depicted in Fig 4.2, is analyzed. If the transmitter and receiver are located in point A and point D, respectively, it is seen that, the communication channel consists of one branching point where 3 cables are connected. Cable lengths are represented with l_1, l_2, l_3 and

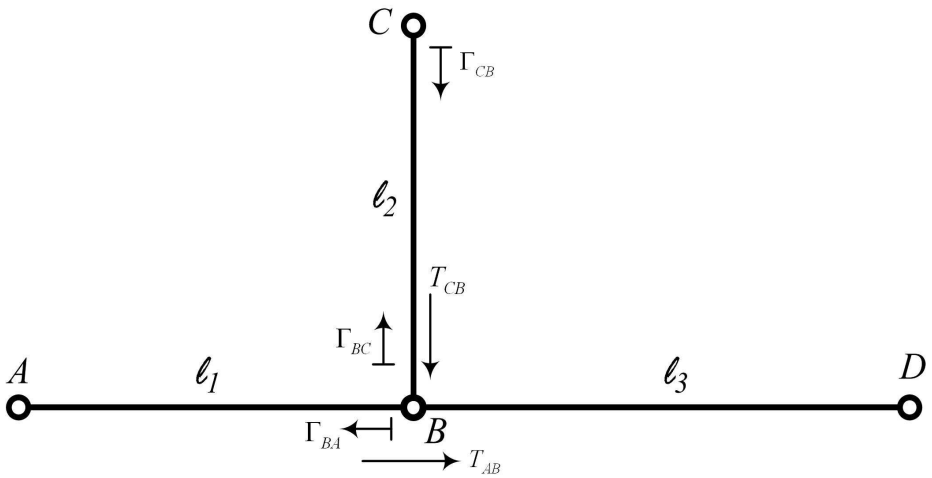

Figure 4.2 Multipath propagation in T network.

characteristic impedance of each cable is $Z_1,\ Z_2,\ Z_3$. The termination load at node C is represented by Z_C. In order to simplify the calculations, input impedances of transmitter and receiver are assumed to be matched to the characteristic impedances of the cables 1 and 3.

$$Z_{transmitter} = Z_1 \quad \text{and} \quad Z_{receiver} = Z_3 \tag{4.9}$$

If a signal leaves node j and reflection occurs at node i and then signal propagation continues backward to node j, the reflection factor at node i is represented as Γ_{ij}. If a signal leaves the node i and a transmission takes place through node j, the transmission coefficient for node j is represented as T_{ji}. So the reflection and transmission coefficients

Table 4.1 Multipath components for T network

	Signal propagating nodes	Reflection factor	Length of propagation
1	$A \rightarrow B \rightarrow D$	T_{AB}	$l_1 + l_3$
2	$A \rightarrow B \rightarrow C \rightarrow B \rightarrow D$	$T_{AB}.\Gamma_{CB}.T_{CB}$	$l_1 + 2l_2 + l_3$
3	$A \rightarrow \big(B \rightarrow C \rightarrow \big)^2 B \rightarrow D$	$T_{AB}.\Gamma_{CB}^2.\Gamma_{BC}.T_{CB}$	$l_1 + 4l_2 + l_3$
$\vdots$	$\vdots$	$\vdots$	$\vdots$
N	$A \rightarrow \big(B \rightarrow C \rightarrow \big)^{N-1} B \rightarrow D$	$T_{AB}.\Gamma_{CB}^{N-1}.\Gamma_{BC}^{N-2}.T_{CB}$	$l_1+2\big(N-1\big)l_2+l_3$

shown in Fig. 4.2 can be calculated as

$$\Gamma_{BA} = \frac{Z_{B_{2-3}} - Z_1}{Z_{B_{2-3}} + Z_1} \qquad \text{where } Z_{B_{2-3}} = Z_2 // Z_3 \tag{4.10}$$

$$\Gamma_{BC} = \frac{Z_{B_{1-3}} - Z_2}{Z_{B_{1-3}} + Z_2} \qquad \text{where } Z_{B_{1-3}} = Z_1 // Z_3 \tag{4.11}$$

$$\Gamma_{CB} = \frac{Z_C - Z_2}{Z_C + Z_2} \tag{4.12}$$

$$\text{and} \tag{4.13}$$

$$T_{CB} = \frac{2Z_{B_{1-3}}}{Z_{B_{1-3}} + Z_2} \tag{4.14}$$

$$T_{AB} = \frac{2Z_{B_{2-3}}}{Z_{B_{2-3}} + Z_2} \tag{4.15}$$

where Z_C represents the load impedance connected to the node C. The N strongest multipath components are listed in Table 4.1.

Consequently, when a signal is transmitted over a PLN, the received signal consists of attenuated, delayed, and phase-shifted version of the transmitted signal. If the total number of received multi-path signals is limited to N, an expression for the frequency response of

the channel can be characterized as follows:

$$H(f) = \sum_{i=1}^{N} \Big\{ \Big[\prod_{k=1}^{K} \Gamma_{ik} \prod_{m=1}^{M} T_{im} \Big] A(f, d_i) e^{-j2\pi f \tau_i} \Big\} \tag{4.16}$$

where $A(f, d_i)$ means the frequency and distance dependent attenuation which will be discussed in the next section.

4.3 Attenuation Analysis

One of the biggest impairments of PLC channels is the increasing signal attenuation with increasing distance and frequency. Attenuation characteristics of power-line cables are studied in literature extensively. Attenuation models are introduced in [38, 39], in these approaches parameters are obtained by measuring the actual PLN. A mathematical formulation is derived in [33], in the proposed method attenuation parameters are calculated individually for each multi-path component.

In order to have a better understanding about attenuation in PLNs, several measurements with different lengths of cables at a particular frequency range were carried out in this study. Its dependency on both frequency and length is investigated. The cable type which is widely available in the PLNs established in Turkey, was used in the measurements. The cross-section of the measured cable is depicted in Fig.4.3. Measurement campaigns were performed by using Agilent vector network analyzer (VNA). The measured frequency range was from 30kHz to 30MHz and cables with length of 10m, 15m, 25m, 40m, 50m, 65m, 75m, 90m, 100m, and 200m were examined.

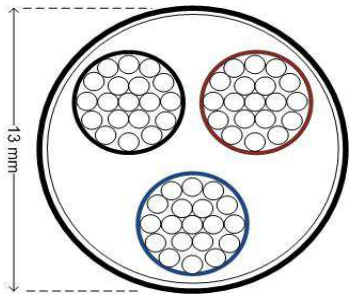

Figure 4.3 Multi-core cable with copper conductor

In this approach, the attenuation values of the cables with different lengths were considered. In this way, several measurements which exhibit the attenuation tendency in different lengths of cable at particular frequencies were obtained. At each frequency, the values were fitted via least square fitting. Consequently, a constant attenuation value was obtained for every frequency, namely unit length attenuation profile (ULAP) which basically reveals the attenuation of the cable per meter. Attenuation for i^{th} path having a length of d_i meters can be calculated as:

$$A(f, d_i) = d_i \left[20 \log_{10}(\text{ULAP}) \right] \tag{4.17}$$

where $A(f, d_i)$ is the signal attenuation related to the length and frequency. For instance, the comparison of the measured attenuation of a cable with 100m and its estimate obtained from (4.17) is plotted in Fig.4.4. As can be seen, the estimate fits well with the measured results.

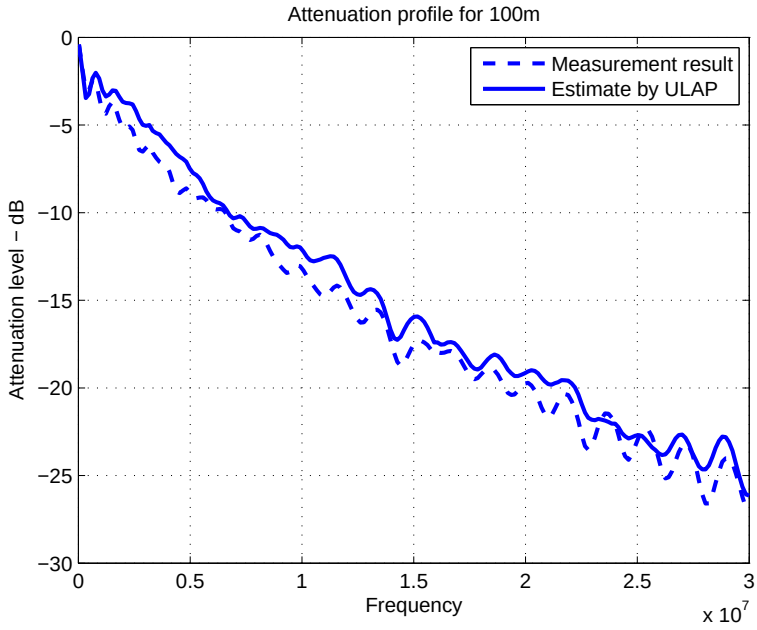

Figure 4.4 Attenuation profile of 100m cable

CHAPTER 5

MULTIPATH SIMULATION ENVIRONMENT

In order to predict the channel characteristics of a particular PLN, a simulation environment is developed to estimate point-to-point channel transfer function within the PLC network. Similar approaches have been proposed in literature for the characterization of the channel transfer function. A simple approach which does not consider multi-path propagation was presented in [39]. With the method proposed, a rough estimation of the transfer function was obtained. A mathematical description of the channel transfer function is introduced in [33], in this approach the calculations of channel parameters for different networks have to be analyzed individually. Besides this, in order to calculate point-to-point transfer function within a PLN, a matrix-based algorithm is presented in [40]. On the other hand, modeling PLC channels as a two-port network model and computing its transfer functions were discussed in [41, 42].

In this section, a simulation environment is introduced. The algorithm considers the PLN topology as a group of matrices where the connection points, reflection and transmission coefficients, termination impedances, and lengths are registered into matrices. Every connection between the nodes and the physical characteristics of the interconnections are represented as set of matrices. Every reflection and transmission coefficient of the network is calculated by computing the input impedances and applied to each multipath component to estimate their reflection coefficients.

5.1 Mapping Network Topology

The algorithm, first, creates the network matrices which contain the information about the connections of the PLC network topology. Every connection between a termination

point, t_i, and branching point, b_i, or between two branching points is entered into the connection matrix CM. It is worth saying that the following assumptions, which are valid for indoor PLNs, are taken into account;

- termination points are connected to a single point,
- there is not any direct connection between the termination points.

$$CM_{\text{mxm}} = \begin{array}{c} \\ t_1 \\ \vdots \\ t_h \\ b_1 \\ \vdots \\ b_k \end{array} \begin{array}{c} \begin{array}{cccccc} t_1 & \dots & t_h & b_1 & \dots & b_k \end{array} \\ \begin{pmatrix} 0 & \dots & 0 & c_{1,h+1} & \dots & c_{1m} \\ \vdots & \ddots & \vdots & \vdots & \ddots & \vdots \\ 0 & \dots & 0 & c_{h,h+1} & \dots & c_{hm} \\ c_{h+1,1} & \dots & c_{h+1,h} & c_{h+1,h+1} & \dots & c_{h+1,m} \\ \vdots & \ddots & \vdots & \vdots & \ddots & \vdots \\ c_{m1} & \dots & c_{mh} & c_{m,h+1} & \dots & c_{mm} \end{pmatrix} \end{array} \tag{5.1}$$

where the total number of termination points is denoted by h, k represents the total number of branching points, and m is the total number of nodes where $m = h + k$. Each element of the connection matrix $CM[m \times m]$ corresponds to an interconnection between two nodes. Since each termination point is connected to a single branching node and no connection exists between termination points the first $[h \times h]$ elements of CM matrix is 0. Therefore, c_{ij} is 1 when there is an interconnection between the corresponding two nodes, otherwise it is 0. The CM matrix exhibits symmetry with respect to its diagonal.

$$c_{ij} = c_{ji} \tag{5.2}$$

So, it is possible to show the CM matrix as;

$$CM_{[(\text{h+k})\text{x}(\text{h+k})]} = \begin{pmatrix} 0_{[h\text{x}h]} & CT_{[h\text{x}k]} \\ CT^T_{[k\text{x}h]} & CB_{[k\text{x}k]} \end{pmatrix} \tag{5.3}$$

where CT matrix describes the interconnections between the termination points and branching points, CB matrix shows the connections among the branching points, and $(\cdot)^T$ represents the transpose of the input matrix. Since no connection exists between the corresponding node and itself, CB matrix is a zero diagonal matrix,

$$CB_{[\mathrm{kxk}]} = \begin{pmatrix} 0 & c_{12} & \dots & c_{1k} \\ c_{21} & 0 & \dots & c_{2k} \\ \vdots & \vdots & \ddots & \vdots \\ c_{k1} & c_{k2} & \dots & 0 \end{pmatrix} \tag{5.4}$$

Lengths of each interconnection between the nodes are entered into an $m \times m$ matrix LM which is generated by replacing the ones in CM matrix with the corresponding lengths. Each length of the interconnections is described with l_{ij}. The length matrix LM can be described as

$$LM_{[(\mathrm{h+k})\mathrm{x}(\mathrm{h+k})]} = \begin{pmatrix} 0_{[h\mathrm{x}h]} & LT_{[h\mathrm{x}k]} \\ LT^T_{[k\mathrm{x}h]} & LB_{[k\mathrm{x}k]} \end{pmatrix} \tag{5.5}$$

where LT corresponds to the length matrix of the cables between termination points and branchings and LB matrix describes the lengths of the cables among the branching points.

5.2 Path Selection

In order to determine the possible paths from the transmitter to the receiver within a PLC network, a new matrix P is formed by using the described interconnections in matrix CM. Matrix P can be considered as the summary of matrix CM in which interconnections between corresponding nodes are explicitly indicated. This step avoids the use of matrix CM whose dimensions become significantly large as the network topology grows complicated. Additionally, a random-path selector is generated. The random-path selector determines the propagating path for each replica of the signal starting from the transmitter until it reaches the receiver. Nodes determined by the random-path selector routine are put in order considering the node labels of transmitter-receiver pairs. Each of these node sequences

corresponds to one of the propagation paths between transmitter and receiver that is to be considered in the derivation of (4.16). The length of these node sequences is calculated by considering the interconnection lengths among nodes of interest. Besides, after defining total length of the propagation path, attenuation for each path is computed using (4.17).

It is possible to find infinitely number of different multipath components even for a small PLN. However, only L number of multipath components make relevant contributions to the overall transfer function of the PLC channel. These L mutipath components are regarded as significant paths. The selection criteria of significant paths is based on setting a power threshold value. The comparison is made with the first received multipath component which is the most powerful one among all the other replicas. The threshold value is set to 30dB;

$$10\log_{10}\frac{|h_0|^2}{|h_i|^2} \geq 30 \tag{5.6}$$

where h_0 and h_i corresponds to the first and the ith paths, respectively, and $|\cdot|^2$ represents the power magnitude.

5.3 Reflection Coefficients

The next step of the proposed algorithm is calculating the transmission and reflection coefficients for each node. Moreover, the total reflection factors for each path is computed. Reflection and transmission coefficients are calculated using (4.5), respectively. At a termination node, load impedance Z_L is equal to the termination point impedance Z_{d_i}. Additionally, reflection/transmission coefficient at a termination node can be computed as it is described in (4.5).

However at a branching node, Z_L is based on treating each branch extending from the node as parallel connection. If a homogeneous network is assumed, the impedance seen by the incident signal arriving at a branching node is given by the following expression:

$$Z_L = \frac{Z_0}{n_i - 1} \tag{5.7}$$

where n_i is the total number of branches extending from a node. Using (5.7), reflection and transmission coefficients for the respective branching nodes can be calculated as:

$$\Gamma_i = \frac{2 - n_i}{n_i} \text{ and } T_i = \Gamma_i + 1 = \frac{2}{n_i} \tag{5.8}$$

Consequently, the matrix R_Γ, whose elements expresses the reflection coefficient for each node, is defined as:

$$R = \begin{array}{c} \begin{matrix} t_1 & \dots & t_h & b_1 & \dots & b_k \end{matrix} \\ \begin{pmatrix} \Gamma_1 & \dots & \Gamma_h & \Gamma_{h+1} & \dots & \Gamma_m \end{pmatrix} \end{array} \tag{5.9}$$

and the transmission coefficient matrix T_T is formed as:

$$T = \begin{array}{c} \begin{matrix} t_1 & \dots & t_h & b_1 & \dots & b_k \end{matrix} \\ \begin{pmatrix} T_1 & \dots & T_h & T_{h+1} & \dots & T_m \end{pmatrix} \end{array} \tag{5.10}$$

It is worth mentioning that characteristic impedance and load impedances are mostly frequency dependent values. However, since no statistical information regarding the impedances is available, they are assumed to be constant steady-state impedance values for all frequencies. In order to calculate the reflection factor for each multi-path component, the propagation path node sequence is used to determine the appropriate transmission/reflection coefficients. The process continues with calculation of channel transfer function $H(f)$ given by (4.16). By applying the inverse fast Fourier transform (IFFT) operation on channel frequency response, channel impulse response is obtained as follows

$$h(\tau) = \sum_{i=0}^{N} h_i \delta(t - \tau_i) \tag{5.11}$$

where τ_i denotes the delay of the ith arriving path.

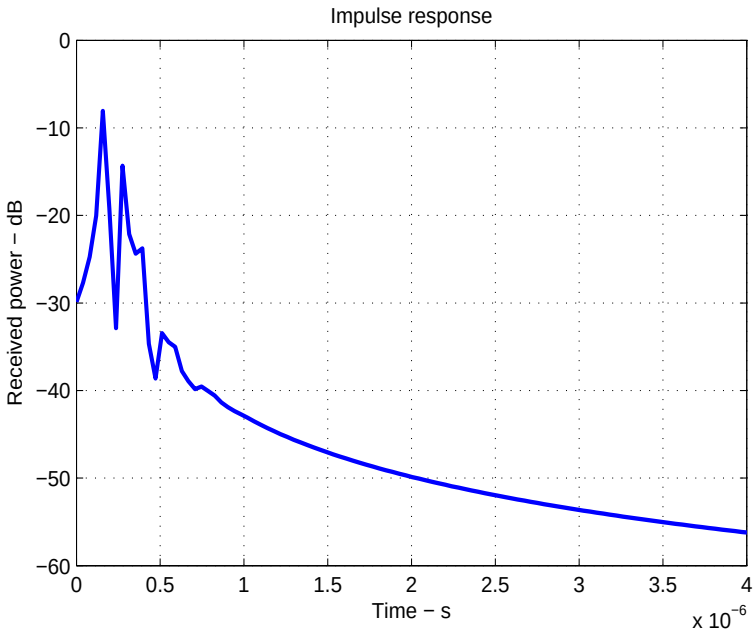

Figure 5.1 Impulse response of the channel between A and D

5.4 Simulation Results

In order to evaluate the simulation results, firstly, a simple T network, which was depicted in 4.2, is analyzed. The transmitter is located in position A and the receiver at D and they are both matched to the characteristic impedances of the cables. It is assumed that the network consists of one type of cable and the characteristic impedance of this specific cable is 100Ω. The termination point C left open and the load impedance Z_L was represented as $10^8\Omega$ in the simulations. Lengths of the cables l_1, l_2, and l_3 are determined as 15m, 10m, and 15m, respectively. The simulation results are depicted in Fig. 5.1, Fig. 5.2(a), and Fig. 5.2(b).

The 5 strongest paths are defined in Table 5.1. Due to the reflections occurred at the open termination point, multipath components are received periodically. Received components can also be identified from the impulse response, as well. The resulting frequency response of the channel is shown in Fig. 5.2(a). Deep notches are observed around 4.5MHz, 13.5MHz, and 22.5MHz.

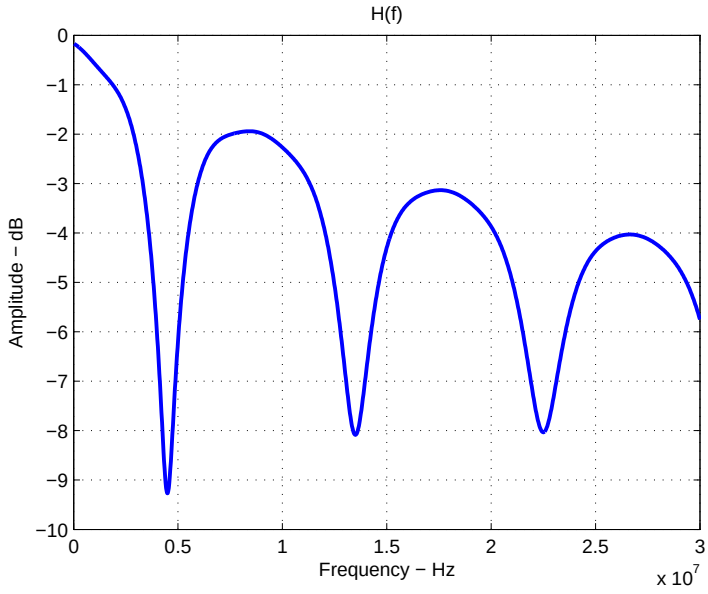

(a) Frequency response

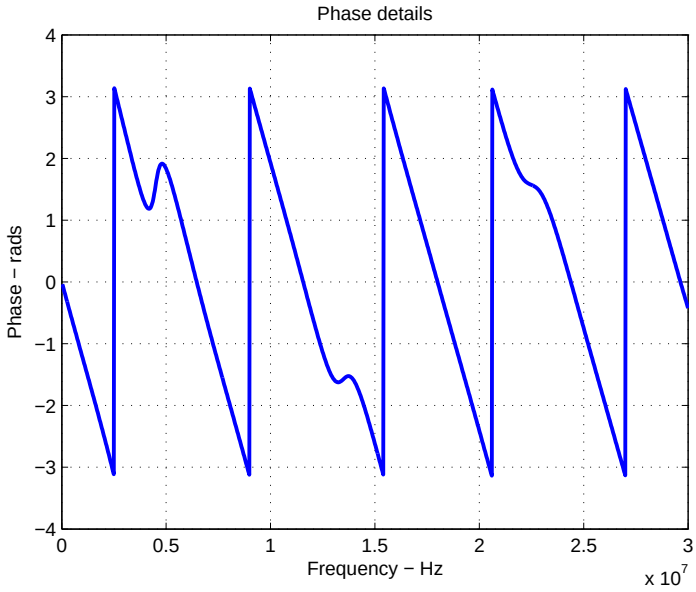

(b) Phase details

Figure 5.2 Frequency response and phase details of the channel between node A and D

5.4.1 Effect of Physical Topology on PLC Channels

In this section, the effect of the physical topology of the power line medium on the communication channel is investigated.

Table 5.1 Multipath components for T network

Paths	Reflection factor	Length of propagation (m)
1	0.6667	30
2	0.4444	50
3	−0.1481	70
4	0.0494	90
5	−0.0165	110

5.4.1.1 Length Between Transmitter and Receiver

In order to understand the effect of the separation between the transmitter and receiver on the PLC channel, the T-network topology, depicted in Fig. 4.2, is analyzed. Length of the branch l_2 was kept constant at 10m and the termination point at node C was left open for the simulations. Length between the transmitter and receiver was varied as 25m, 50m, 100m, and 200m. The branching point B was connected at the midpoint for every simulation. Channel impulse responses and transfer functions are shown in Fig. 5.3(a) and Fig. 5.3(b), respectively.

From Fig.5.3(a), since delays between multipath components are related to the length of the branch, delays between the first coming path and the others do not change with the distance between transmitter and receiver changes. However, due to the attenuation, distortion increases and the shape of the channel impulse response loses its original shape.

Transfer functions are depicted in Fig.5.3(b). As can be seen, the notches do not vary with either frequency or line length. The reason for that is the delays of the multipath components are not related to the distance between transmitter and receiver. The main factor that can change the delays is the length of the branch BC. Additionally, attenuation tends to increase as the distance and frequency increase.

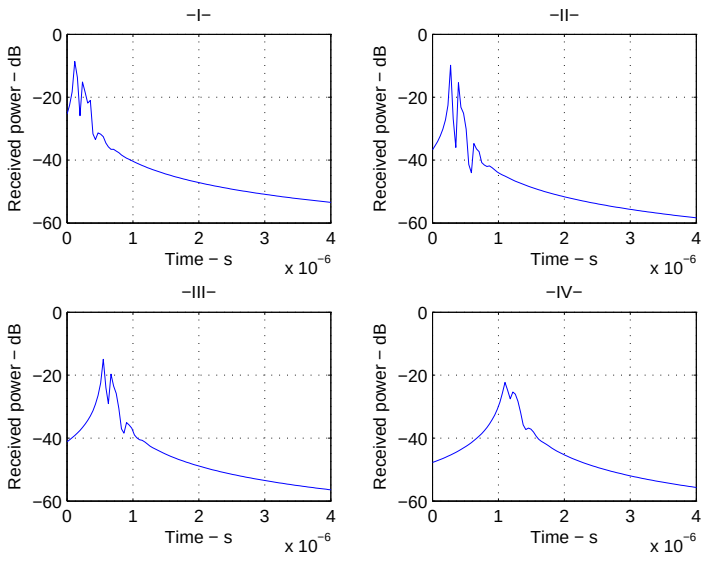

(a) Impulse response

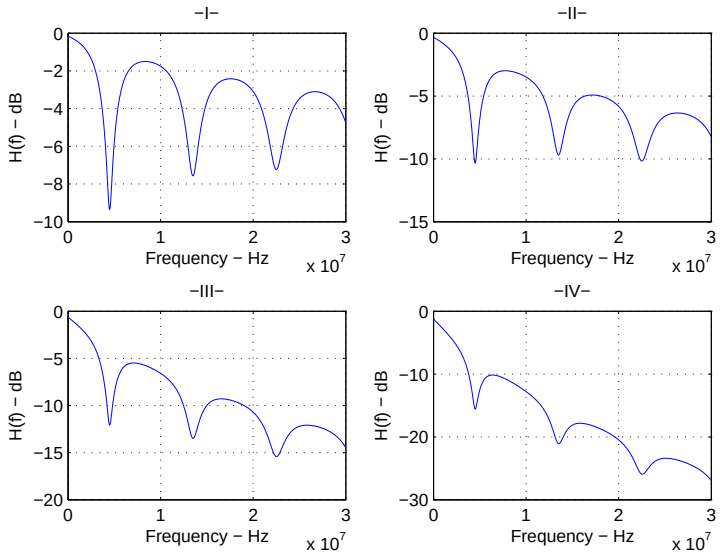

(b) Frequency response

Figure 5.3 Impulse and frequency response for different distances between transmitter and receiver; (I)25m, (II)50m, (III)100m, and (IV)200m

5.4.1.2 Length of Branch

In order to understand the effect of the length of the branch on both the transfer function and channel impulse response, the topology used previously, which was depicted in Fig.4.2, is used. The length of the branch BC was varied at 5m, 10m, 15m, and 20m, while the

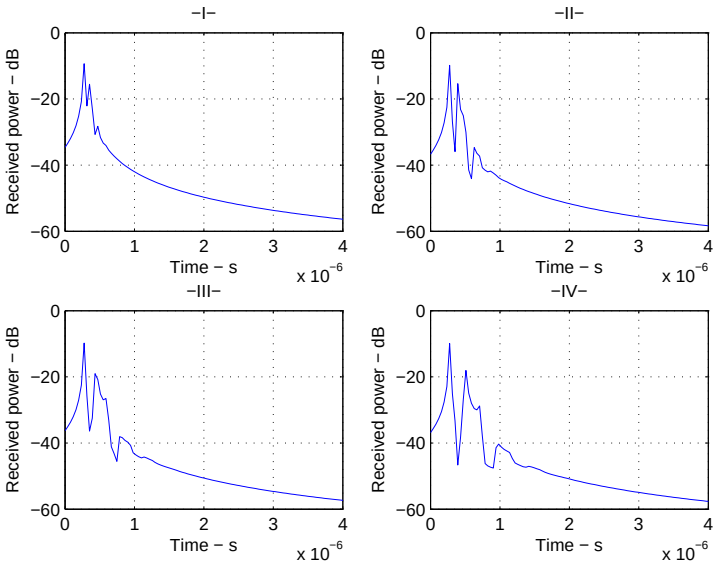

(a) Impulse response

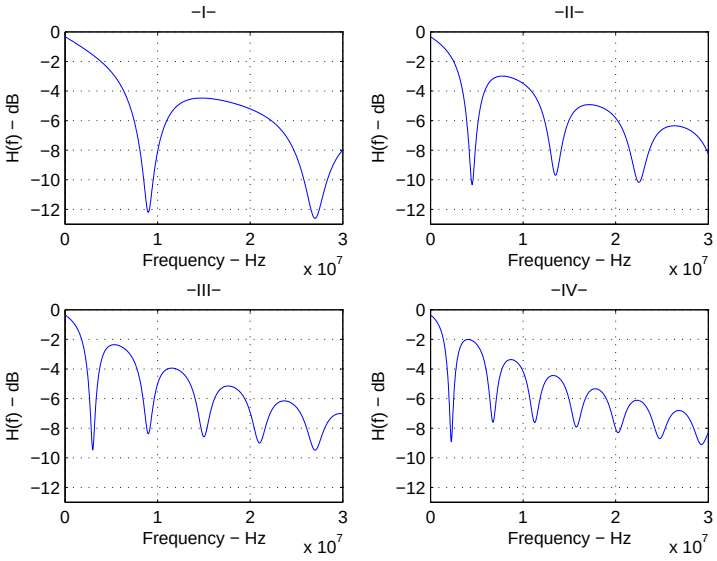

(b) Frequency response

Figure 5.4 Impulse and frequency response for different lengths of branch; (I)5m, (II)10m, (III)15m, and (IV)20m

distance between transmitter and receiver was kept constant at 50m and node C was left open. Results are shown in Fig.5.4(a) and Fig.5.4(b).

As can be seen from Fig.5.4(a), with the increment in the length of branch BC, delay and attenuation values for each received multipath component increase, while the delay

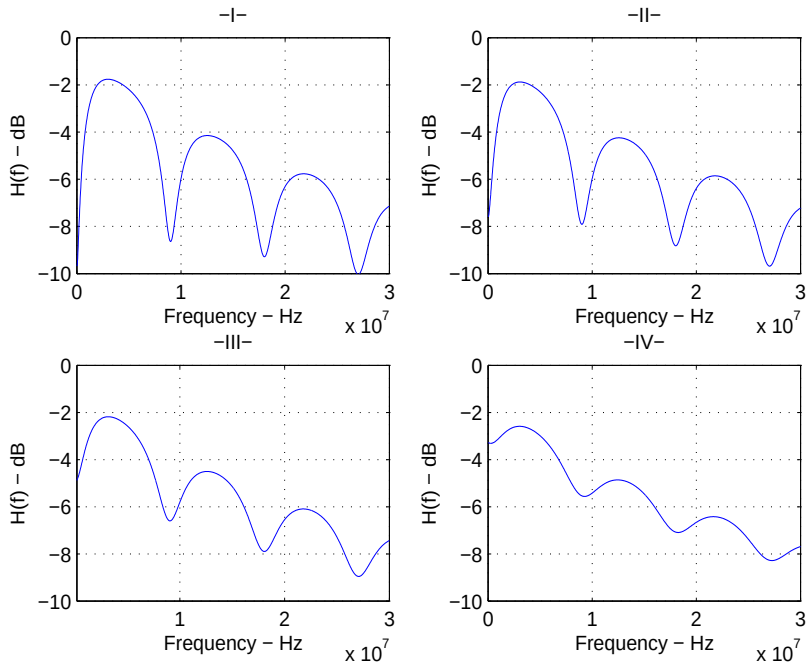

Figure 5.5 Channel frequency responses for different load impedance values; (I)5Ω, (II)10Ω, (III)25Ω, and (IV)50Ω

and the power of the first received path remains constant. Any change in the delays cause changes in the position of the notches detected in transfer functions. From Fig.5.4(b), it is observed that, with any increment in the length of the branch BC, number of notches, detected in a particular frequency range, increases.

Since the position of the notches in frequency domain depend on the length of the branch, a generalized expression can be given;

$$f_N = \frac{45}{L}(2n+1) \quad \text{for} \quad n = 0, 1, 2, ... \tag{5.12}$$

where L represents the length of the branch BC in meter and the result is in MHz.

5.4.1.3 Load Impedance

In this section, the effect of the load impedance on channel transfer function is analyzed. As described previously, characteristic impedance Z_0 of the cable is assumed to be 100Ω

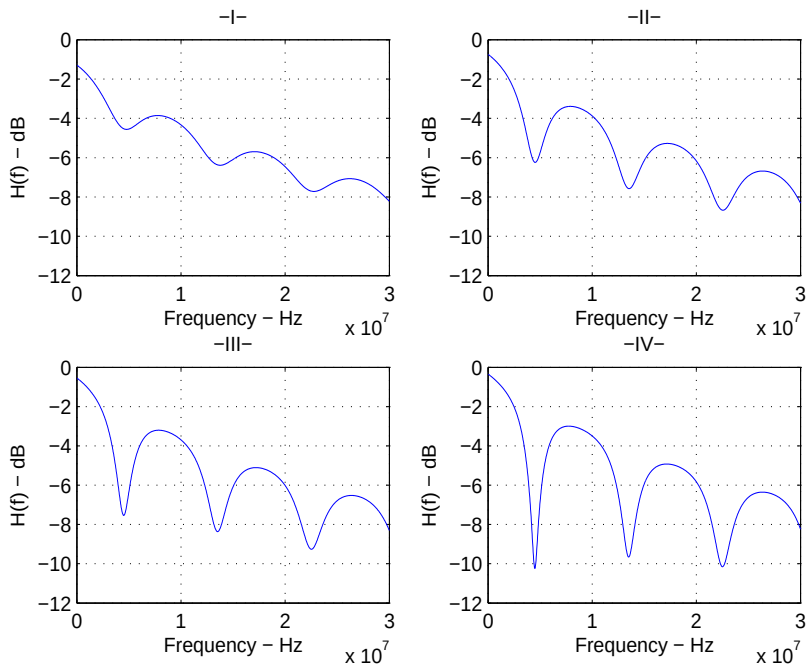

Figure 5.6 Channel frequency responses for different load impedance values; (I)200Ω, (II)50Ω, (III)1kΩ, and (IV)50kΩ

in the simulations. Here, influence of load impedances is analyzed by two different set of impedance values, which can be grouped as

- Loads lower than Z_0:

  In order to see the effect of load impedance, the T-network topology, which has been used for the previous simulations, was used. Distance between transmitter and receiver was kept constant at 50m and length of the branching was 10m. Load impedance values were defined as 5Ω, 10Ω, 25Ω, and 50Ω. Transfer functions are shown in Fig.5.5.

  Since reflection coefficient Γ_{CB} increases as the load impedance increases toward Z_0, reflected multipath components attenuate less. Thus, stronger multipath components will be received. This leads to an increment in the depth of the notches in transfer functions.

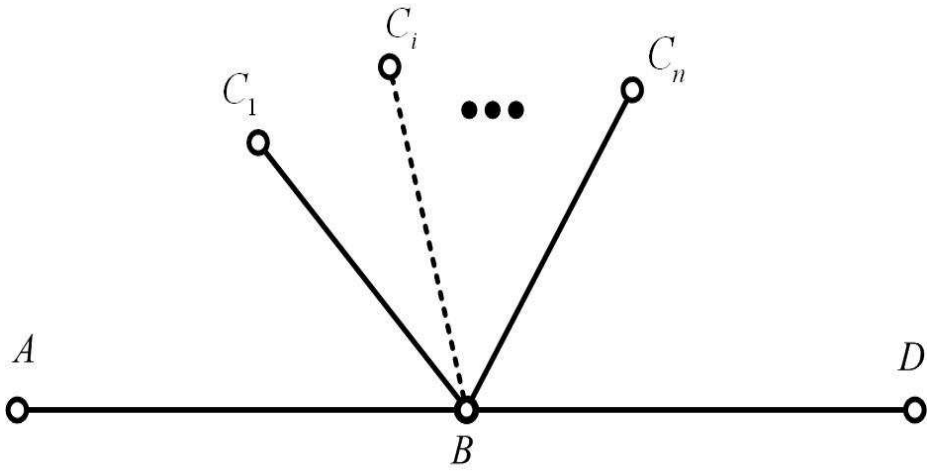

Figure 5.7 T network with multiple branchings distributed from single node

- Loads higher than Z_0:

  In order to see the effect of load impedances higher than Z_0, the T-network topology was used. Distance between transmitter and receiver was kept constant at 50m and length of the branching was 10m. Load impedance values were defined as 200Ω, 500Ω, 1kΩ, and 50kΩ. Transfer functions are shown in Fig.5.6.

  Since reflection coefficient Γ_{CB} increases as the load impedance tends to get higher values than Z_0, reflected multipath components attenuate less. Thus, stronger multipath components will be received. This leads to an increment in the depth of the notches in transfer functions. As can be seen from Fig.5.6, notches become more prominent with higher values of load impedance.

5.4.1.4 Number of Branchings

In this section, number of branchings which are distributed from a single node, as depicted in Fig.5.7, is analyzed. Number of branches were defined as 2, 3, 4, and 5. Distance between transmitter and receiver and length of branches were set to 100m and 10m, respectively. Branches were ended with open circuits.

Fig.5.8(a) shows the channel impulse responses for all cases. It is seen that, increasing the number of branches, which are connected at the same node, increases the attenua-

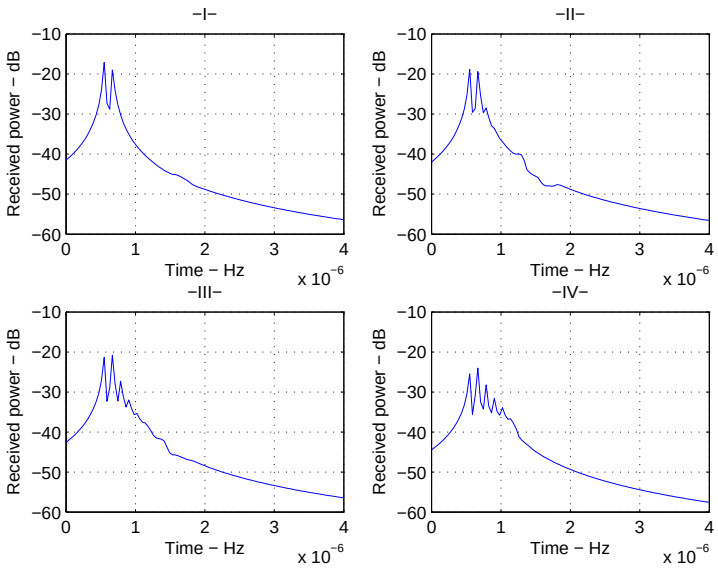

(a) Impulse response

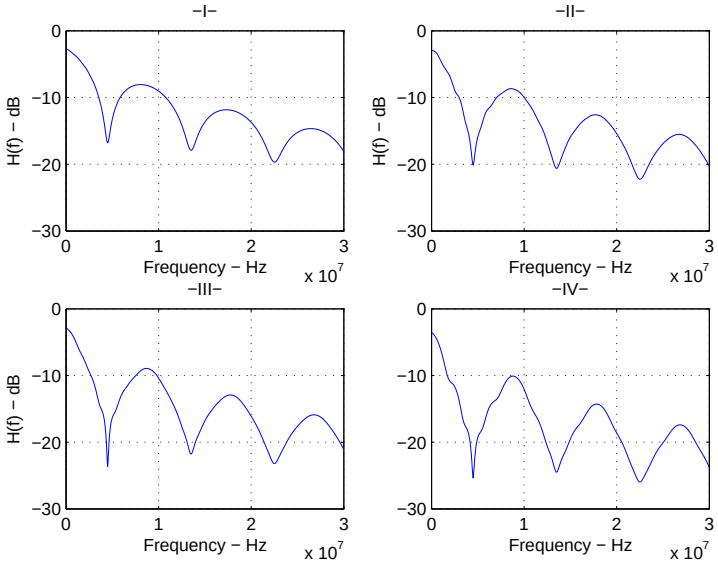

(b) Frequency response

Figure 5.8 Impulse and frequency response for multiple branches connected at the single node; (I)two branches, (II)three branches, (III)five branches, and (IV)ten branches

tion. However, by increasing the number of branches, it is also observed that, subsequent multipath components are becoming stronger.

Transfer functions of the channels are depicted in Fig.5.8(b). As can be seen from the figures, although the sharpness of the notches decreases while number of branches increases, depths and widths of the notches are increasing.

5.5 Channel Characterization

Multipath characteristics of PLC channels are described by their impulse response. For PLC systems, channel impulse response is highly related to the topology and the characteristics of the PLN. In order to compare different multipath channel characteristics, different delay parameters must be used. Due to the multipath signal propagation, inter-symbol interference (ISI) may occur during the data transmission. The root-mean-squared (RMS) delay spread and maximum excess delay spread are the multipath channel parameters that can be derived from channel impulse responses [43]. These delay spread parameters are very necessary for determining limits of the channel ISI for improvements of modulation schemes.

The RMS delay spread describes the capability of the communication channel of supporting high data rate communications by implying the probability of performance degradation because of the ISI effect. It is calculated as taking the square root of the second central moment of the power delay profile and is defined to be

$$\sigma_\tau = \sqrt{\bar{\tau^2} - (\bar{\tau})^2} \tag{5.13}$$

where

$$\bar{\tau^2} = \frac{\sum_k^R a_k^2 \tau_k^2}{\sum_k^R a_k^2} = \frac{\sum_k^R P(\tau_k)\tau_k^2}{\sum_k^R P(\tau_k)} \tag{5.14}$$

$$\bar{\tau} = \frac{\sum_k^R a_k^2 \tau_k}{\sum_k^R a_k^2} = \frac{\sum_k^R P(\tau_k)\tau_k}{\sum_k^R P(\tau_k)} \tag{5.15}$$

$$P(\tau) = \left|h(t,\tau)\right|^2 \tag{5.16}$$

where the RMS delay spread is denoted by σ_τ and R is the number of paths considered in the calculations. R is determined by applying a threshold considering the maximum value of the received multipath components. τ_k represents the delay of the kth multipath component. Delays are measured relative to the first detectable signal arriving at the receiver $\tau_0 = 0$. The complex amplitude value of the received multipath component arriving with a delay of τ_k is shown with $h(t, \tau_k)$ in the equation.

The maximum excess delay (X dB) of the power delay profile is defined as the relative time delay from the first arrived multipath to the last multipath component that falls to X dB below the maximum one. If τ_0 represents the first arriving multipath component and τ_X is the delay of the last multipath component which is still within X dB of the strongest arriving multipath signal, then maximum excess delay can be calculated as

$$\rho_{X\text{dB}} = \tau_X - \tau_0 \tag{5.17}$$

where $\rho_{X\text{dB}}$ represents the maximum excess delay with a threshold value of X dB. Please note that, it is not necessary to receive the strongest amplitude value at τ_0. With respect to these definitions, the threshold value for both RMS delay spread and maximum excess delay is set to 20dB.

In order to understand the effect of the network topology on the channel characterization parameters, different PLN topologies are generated. The generic form of the PLN topology is illustrated in Fig. 5.9. In this section, impact of loading at termination nodes and number of branching nodes between transmitter and receiver is analyzed. Impedance values of termination points were varied as characteristic impedance, 250Ω, 2500Ω, and open circuit. The network is considered with two, four and six branches in the link between sending and receiving ends. For each network topology, different power delay profiles with different termination loads are analyzed.

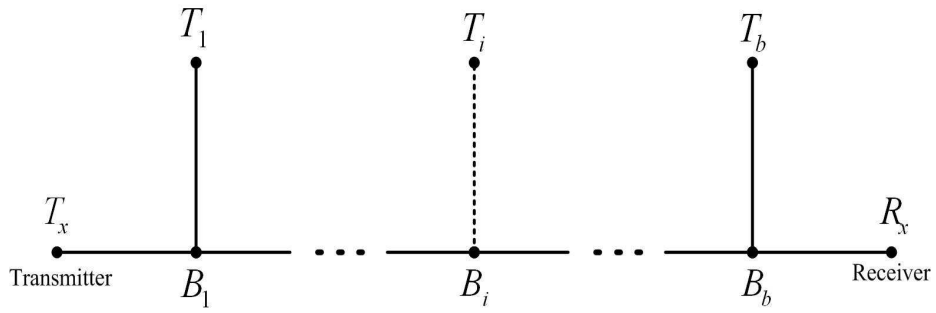

Figure 5.9 Graphical illustration of then PLC network topology considered in this section

Table 5.2 Channel parameters for the network with two branches

Branch Loads	σ_τ (in μs)	$\rho_{20\text{dB}}$ (in μs)
Char. Imp.	0.0741	0.2
250Ω	0.1457	0.4333
2500Ω	0.1847	0.4667
Open circuit	0.1896	0.4667

5.5.1 PLN with Two Branches

Consider the PLN topology that is depicted in Fig. 5.9 with two branches between transmitter and receiver. The distance from transmitter to receiver was kept constant at 100m and length of each branch was determined as 10m. Please note that, the branches were equally distributed between transmitter T_x and receiver R_x. Simulation results are depicted in Fig. 5.10 for four different loading cases. The channel characterization parameters, namely, RMS delay spread and maximum excess delays are shown in Table.5.2. It is seen from the results that, for the case of termination loadings are equal to characteristic impedance, both RMS delay spread and maximum excess delay have the lowest value. Any increment in the loading impedances increase the delay parameter values. The reason can be explained as, the multipath components, which are returning from the termination points, are becoming stronger when the termination loading values are increasing toward the characteristic impedance. So more powerful multipath components are received in the

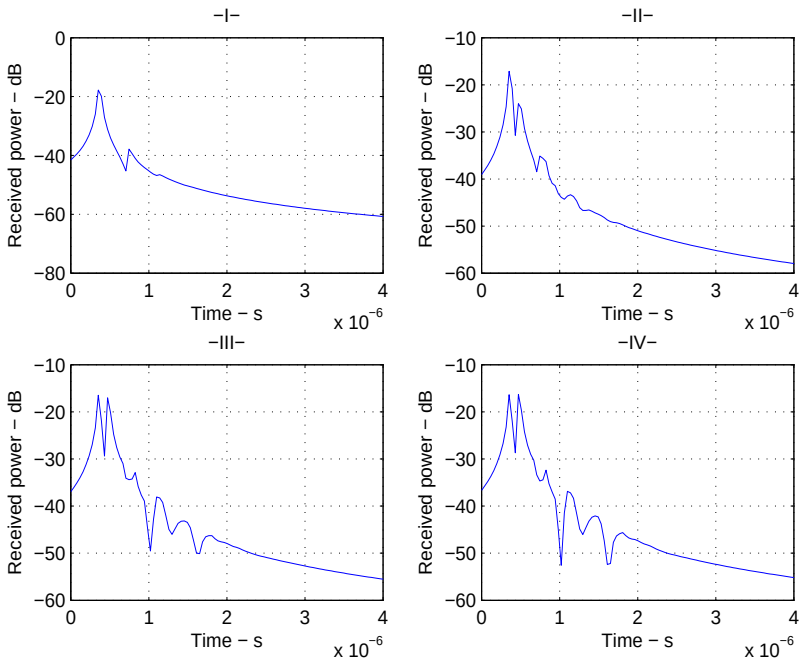

Figure 5.10 Simulated power delay profiles for the PLN with two branches and all terminated in (I)characteristic impedance, (II)250Ω, (II)2500Ω, and (IV)open circuit

Table 5.3 Channel parameters for the network with four branches

Branch Loads	σ_τ (in μs)	$\rho_{20\text{dB}}$ (in μs)
Char. Imp.	0.1434	0.4333
250Ω	0.2403	0.5
2500Ω	0.3882	0.6333
Open circuit	0.4189	0.6667

receiver which leads to an increment in the delay parameter values. It is observed that the highest values among the delay parameter values are observed for the short circuit case.

5.5.2 PLN with Four Branches

Consider the PLN topology that is depicted in Fig. 5.9 with four branches between transmitter and receiver. The distance from transmitter to receiver was kept constant at 100m

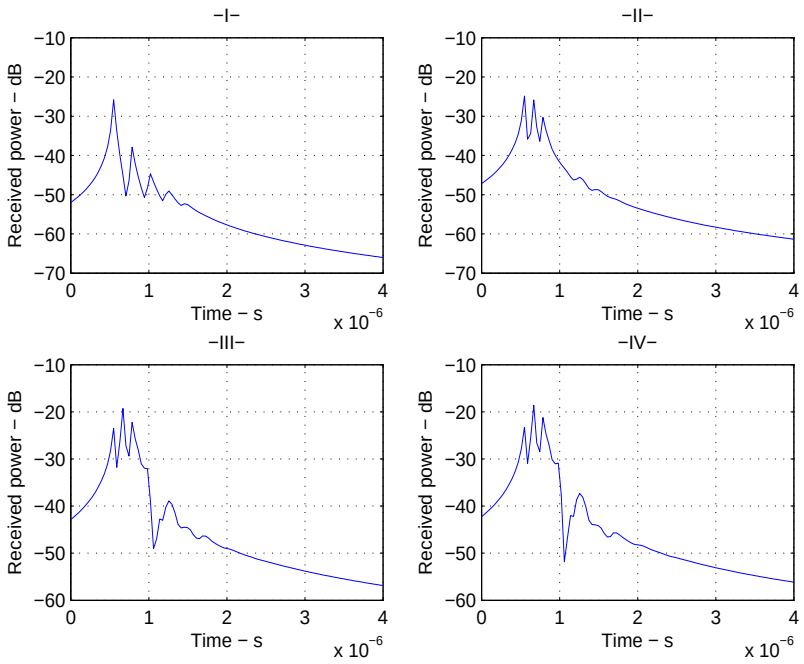

Figure 5.11 Simulated power delay profiles for the PLN with four branches and all terminated in (I)characteristic impedance, (II)250Ω, (II)2500Ω, and (IV)open circuit

and length of each branch was determined as 10m. The branches were equally distributed between transmitter T_x and receiver R_x. Simulation results are depicted in Fig. 5.11 for four different loading cases. The channel characterization parameters, namely, RMS delay spread and maximum excess delays are shown in Table.5.3. It is seen from the results that, for the case of termination loadings are equal to characteristic impedance, both RMS delay spread and maximum excess delay have the lowest value. Any increment in the loading impedances increase the delay parameter values. The reason can be explained as, the multipath components, which are returning from the termination points, are becoming stronger when the termination loading values are increasing toward the characteristic impedance. So more powerful multipath components are received in the receiver which leads to an increment in the delay parameter values. It is observed that the highest values among the delay parameter values are observed for the short circuit case.

Table 5.4 Channel parameters for the network with six branches

Branch Loads	σ_τ (in μs)	$\rho_{20\text{dB}}$ (in μs)
Char. Imp.	0.2288	0.6
250Ω	0.4479	0.7
2500Ω	0.6326	0.7333
Open circuit	0.6572	0.7333

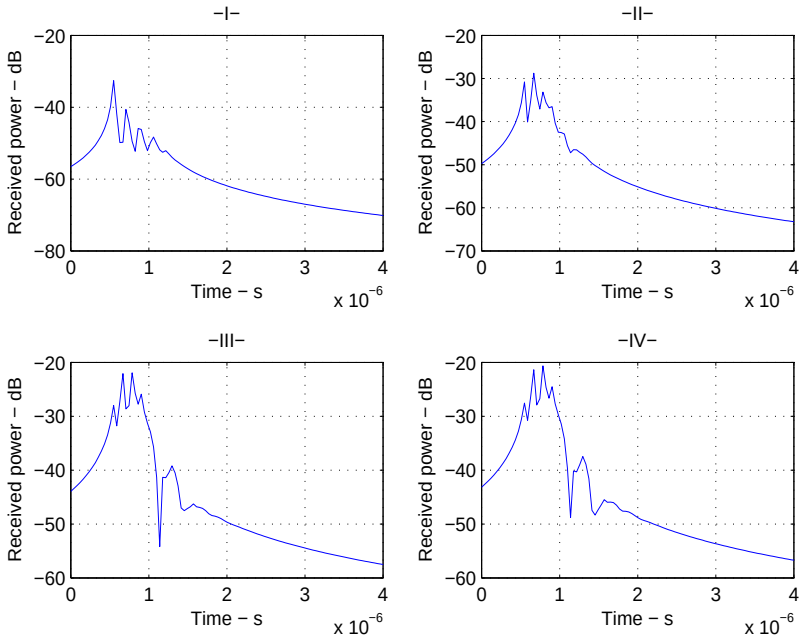

Figure 5.12 Simulated power delay profiles for the PLN with four branches and all terminated in (I)characteristic impedance, (II)250Ω, (II)2500Ω, and (IV)open circuit

5.5.3 PLN with Six Branches

Consider the PLN topology that is depicted in Fig. 5.9 with six branches between transmitter and receiver. The distance from transmitter to receiver was kept constant at 100m and length of each branch was determined as 10m. Please note that, the branches were equally distributed between transmitter T_x and receiver R_x. Simulation results are depicted in Fig. 5.12 for four different loading cases. The channel characterization param-

eters, namely, RMS delay spread and maximum excess delays are shown in Table.5.4. It is seen from the results that, for the case of termination loadings are equal to characteristic impedance, both RMS delay spread and maximum excess delay have the lowest value. Any increment in the loading impedances increase the delay parameter values. The reason can be explained as, the multipath components, which are returning from the termination points, are becoming stronger when the termination loading values are increasing toward the characteristic impedance. So more powerful multipath components are received in the receiver which leads to an increment in the delay parameter values. It is observed that the highest values among the delay parameter values are observed for the short circuit case.

5.6 Statistical Analysis

PLC systems may have entirely different physical characteristics. Due to this several distinct topology features, delay parameters may vary extensively. Up to now, however, PLC channel characterization process has been done for specific topologies [33, 34, 40, 44–53]. However, in order to design reliable communication systems, which can work in every desired channel, analyzing the channel parameters statistically is very important. In this section, instead of analyzing the results of some specific PLN topologies, results of several different PLN topologies will be analyzed statistically.

Among the several different physical characteristics of PLNs, impact of the following items on the delay spread parameters, namely, RMS delay spread and maximum excess delay (20dB), will be examined in this section:

- distance between transmitter and receiver
- number of branching nodes between transmitter and receiver
- length statistics of branches

In order to analyze these parameters, more complicated PLN topologies are formed as depicted in Fig. 5.13 where nodes denoted by B and T are branching and termination points, respectively. The total number of branching points between transmitter and receiver

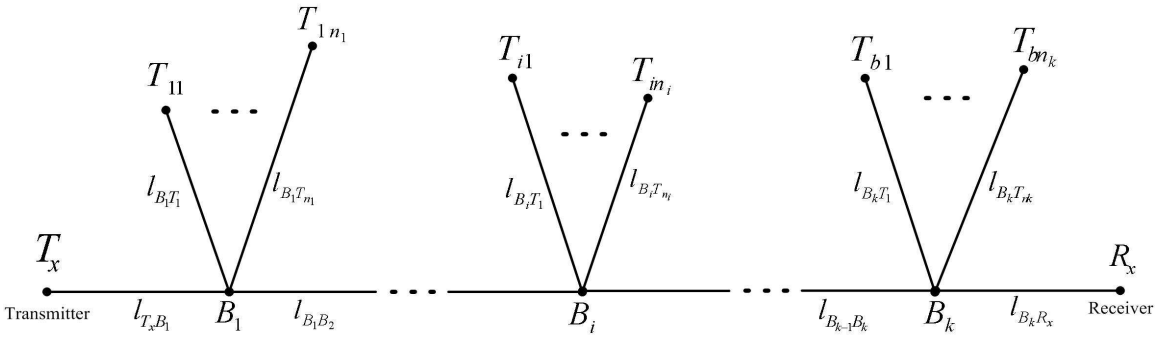

Figure 5.13 Graphical illustration of then PLC network topology considered in this section

is denoted by k. Number of branches distributed from ith branching point is shown by n_i and length of the cable between node x and y is shown by l_{xy}.

As shown in the previous section and analyzed in [44, 45], delay spread parameters take the maximum values where termination loadings are terminated in very low impedances or very high impedances which are closer to infinity. In order to consider the worst case scenarios for all the PLN topologies and solely focus on the topics listed above, all the termination points are assumed to be open circuits [54].

In this analysis, matrix based PLC simulation technique proposed in Section 5.1 will be considered. However, matrices are modified in a way that the simulation module lets us generate random PLC networks with different physical characteristics. At the same time, the simulation environment still gives us the control of the specific parameters of the physical topology which the focus is on. The topology of the network is generated by generating different connection matrices

$$\mathbf{C}_{[(h+2+k)\mathrm{x}(h+2+k)]} = \begin{pmatrix} 0_{[(h+2)\mathrm{x}(h+2)]} & CT_{[(h+2)\mathrm{x}k]} \\ CT^T_{[k\mathrm{x}(h+2)]} & CB_{[k\mathrm{x}k]} \end{pmatrix} \tag{5.18}$$

where CT matrix describes the interconnections between the termination points and branching points, CB matrix shows the connections among the branching points. Total number of termination points and the total number of branching points are described by h and k, respectively. The number "2" comes from the interconnections of transmitter and receiver to the PLN. Number of branches extending from each branching point is uniformly

distributed over [1,4] in the simulations. Characteristic impedance of the cables is set to 100Ω and transmitter and receiver are also assumed to be matched to the characteristic impedance. Impact of physical attributes is statistically investigated by generating 20000 realizations of PLC network for each case taken into account.

Different PLC topologies with different physical attributes are generated by manipulating the values of h, k, and lengths of interconnections l_{xy}. Difference on h and k values results in a change in the dimensions of the submatrices denoted as CB and CT. However, it is worth saying that, in order to focus solely on the impact of specific physical characteristics, simulations are performed with constant number of branching points. For example, impact of distance between transmitter and receiver is analyzed where the number of branching points is kept constant at 4 or impact of number of branchings are analyzed by setting constant number of k for each 20000 realizations. Consequently, there is no need to change the CB matrix throughout the simulations for constant branching point number. CB matrix can be shown as

$$CB_{[k\times k]} = \begin{pmatrix} 0 & 1 & 0 & \dots & \dots & \dots & 0 \\ 1 & 0 & 1 & & & & \vdots \\ 0 & 1 & 0 & \ddots & & & \vdots \\ \vdots & & \ddots & \ddots & \ddots & & \vdots \\ \vdots & & & \ddots & 0 & 1 & 0 \\ \vdots & & & & 1 & 0 & 1 \\ 0 & \dots & \dots & \dots & 0 & 1 & 0 \end{pmatrix} \tag{5.19}$$

However, since number of branches distributed from each branching point is uniformly distributed, this case is not valid for CT matrix. Size of CT matrix will be changed with the total number of branches h.

$$h = \sum_{i=1}^{k} n_i \tag{5.20}$$

Please note that, as stated before, each n_i value is uniformly distributed over [1,4]. Thus, mapping of CT matrix can be shown as

$$CT_{[(h+2)\mathrm{x}k]} = \left(\begin{array}{cccc}
1 & 0 & \dots & 0 \\
\hline
0 & 0 & \dots & 1 \\
\hline
1 & 0 & \dots & 0 \\
\vdots & \vdots & \ddots & \vdots \\
1 & 0 & \dots & 0 \\
\hline
0 & 1 & \dots & 0 \\
\vdots & \vdots & \ddots & \vdots \\
0 & 1 & \dots & 0 \\
\hline
\vdots & \vdots & \ddots & \vdots \\
\hline
0 & 0 & \dots & 1 \\
\vdots & \vdots & \ddots & \vdots \\
0 & 0 & \dots & 1
\end{array}\right)
\begin{array}{l}
\Leftarrow T_x - B_1 \text{ connection} \\
\Leftarrow B_k - R_x \text{ connection} \\
\\
\Leftarrow \text{Branches from } B_1 \\
\\
\\
\Leftarrow \text{Branches from } B_2 \\
\\
\Leftarrow \text{Branches from } B_i \\
\\
\Leftarrow \text{Branches from } B_k \\
\\
\end{array} \tag{5.21}$$

where the first and the second rows represent the interconnections from transmitter to node B_1 and from receiver to B_k, respectively. The rest of CT matrix is expressing other connections between the termination nodes and branching points.

As discussed in detail in Section 5.1, the corresponding lengths of each interconnection and impedances at termination points are kept in separate matrices. With any change in the dimensions of CM matrix, dimensions of length and impedance matrices will also change.

The impact of number nodes between transmitter and receiver on RMS delay spread and maximum excess delay can be seen in Fig. 5.14(a). While deriving this figure, distance between transmitter and receiver and length statistics of the branches were considered to be 150m and U[10m − 30m], respectively, where U refers to uniform distribution. Upon the analysis performed, it is concluded that an increase in the number of branching nodes gives rise to an increase in RMS delay spreads value. This behavior can be related to more multipath components received and to the multipath components arriving at larger delays as k increased.

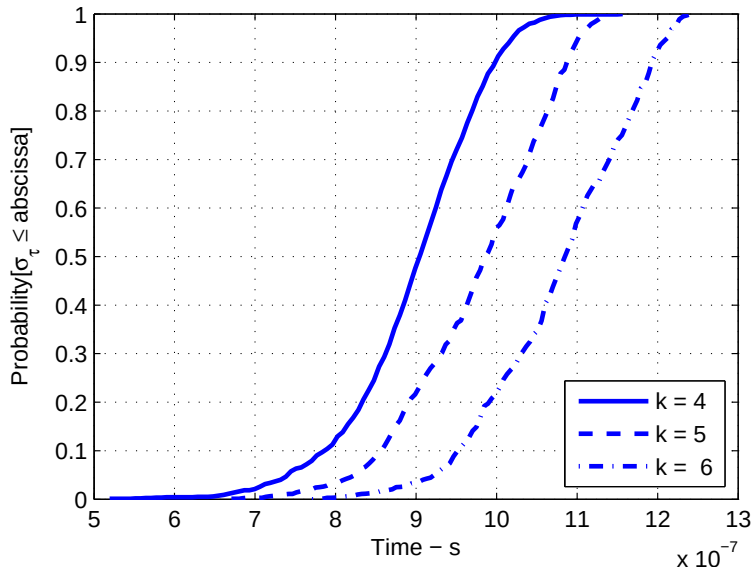

(a) RMS delay spread

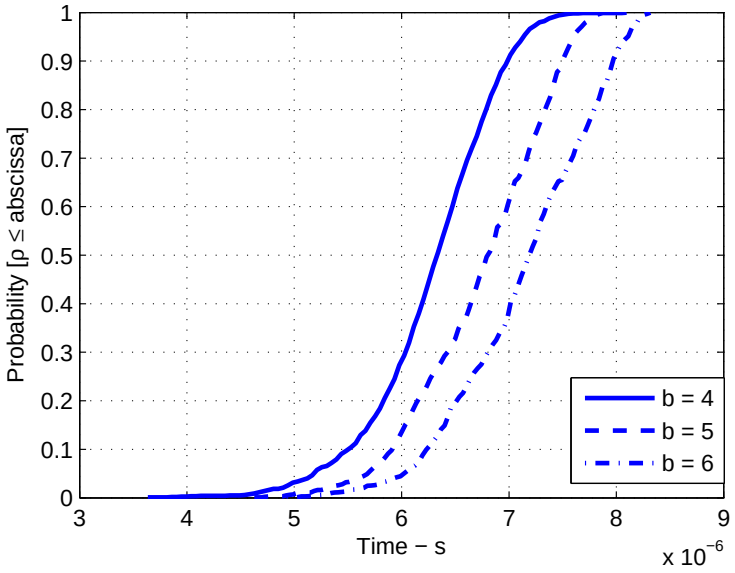

(b) Maximum excess delay

Figure 5.14 Dependency of RMS delay spread (σ_τ) and maximum excess delay (ρ) on the number of branching points k between T_x and R_x

Fig. 5.15(a) and Fig. 5.15(b) show the impact of the distance between transmitter and receiver on RMS delay spread and maximum excess delay. Throughout the simulations, number of branching points between transmitter and receiver was kept constant as 4 and branch lengths are assumed to be uniformly distributed over [10m − 30m]. Similar to the

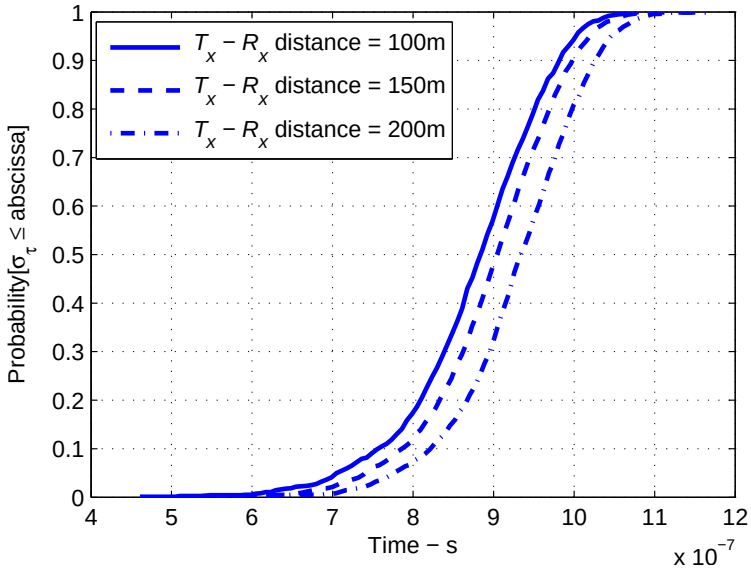

(a) RMS delay spread

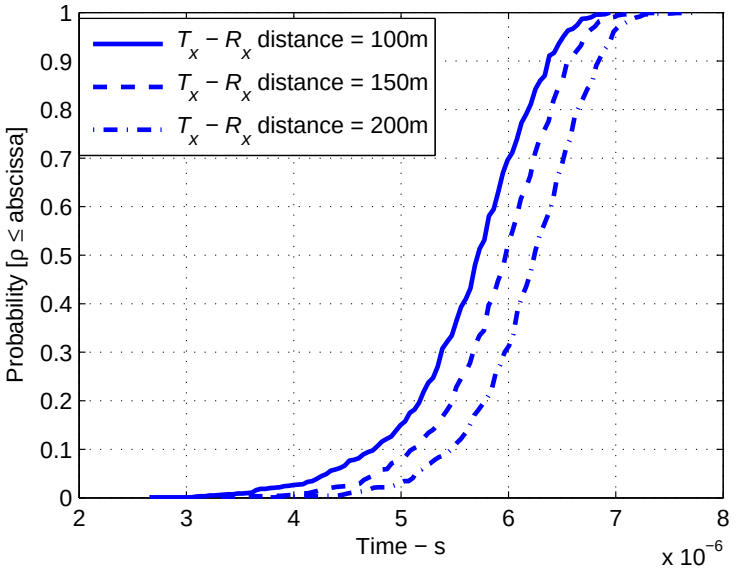

(b) Maximum excess delay

Figure 5.15 Dependency of RMS delay spread (σ_τ) and maximum excess delay (ρ) on the distance between T_x and R_x

previous case analyzed, increasing separation distance between transmitter and receiver leads to the reception of multipath components at larger delays leading to an increase in RMS delay spread and maximum excess delay values.

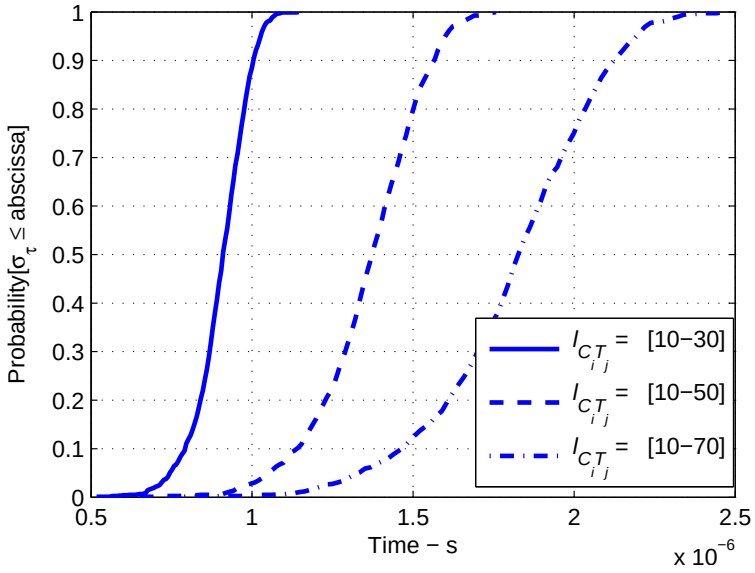

(a) RMS delay spread

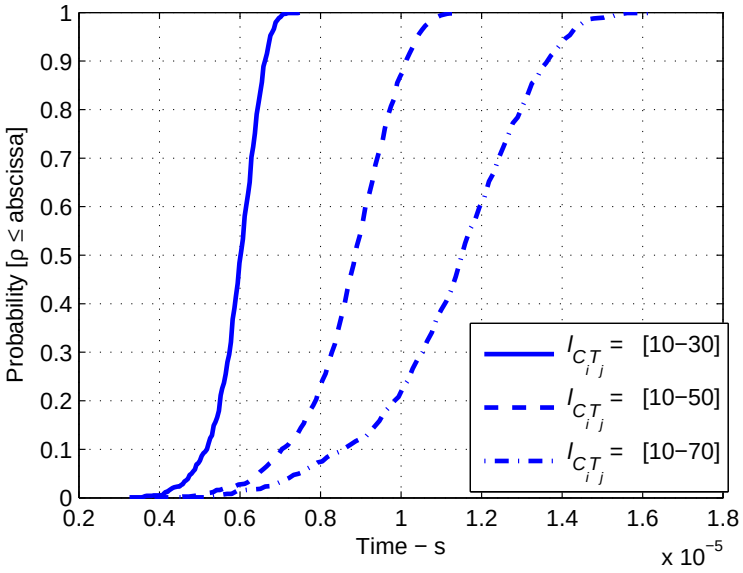

(b) Maximum excess delay

Figure 5.16 Dependency of RMS delay spread (σ_τ) and maximum excess delay (ρ) on the length statistics of branches

Finally, the impact of branch length statistics is seen in Fig. 5.16(a) and Fig. 5.16(b) where the number of branching points between transmitter and receiver was set to 4 and separation distance between transmitter and receiver was 150m. Among all the analyzed factors, change in branch length statistics seems to yield the most drastic change in delay

spread values. The reason for that can be explained as, expanding the range of lengths increase the probability of receiving multipath components with larger delays.

CHAPTER 6

CONCLUSION AND FUTURE WORK

Recently, communication over power lines has been addressed as one of the competitive technology for indoor digital entertainment communication systems. However, design of PLC systems requires a very good understanding of noise, attenuation, and multipath characteristics of the power line channel. This thesis is mainly focused on noise and multipath characteristics of PLC channels within the frequency range between 30kHz and 30MHz.

Noise is regarded as one of the main challenges that has to be addressed for the establishment of reliable PLC based communication systems. Impulsive noise, generated by house appliances connected to the network, being one of the noise types present in PLC systems, needs special attention. In Chapter 2, in order to have a better understanding of noise generated by electrical devices, a novel and reliable measurement setup was established. The effectiveness of the measurement setup was shown. Several electrical home appliances were analyzed and the most significant noise sources have been identified. Their features both in time and frequency are extracted. Peak excursion and maximum power change of each device has been identified. Additionally, the additive effect of noise in PLC channels is investigated.

In Chapter 3, a noise simulation model was introduced. The proposed model takes all the noise sources under consideration and generates each type of noise, namely colored background noise, narrowband noise, and impulsive noise, individually. Results were depicted and discussed.

Mutlipath and attenuation characteristics of PLC channels were investigated in Chapter 4. Reflection and transmission coefficients were derived. Multipath analysis for a T network is done. In order to have a better understanding on attenuation, a reliable measurement

setup was established and the attenuation profile, namely ULAP, has been developed. The estimate values were compared with the measurement results.

In Chapter 5, a matrix based PLC multipath simulation environment was introduced. A unique path selection algorithm was proposed. Channel transfer functions of several simple networks are analyzed with relevant discussions. Effect of

- direct line length between transmitter and receiver,
- length of the branches connected to the PLN,
- number of the branches connected to a single node along the direct line,
- impedance values seen at termination nodes,

were investigated. Important relations between the above mentioned physical attributes and the channel transfer functions are drawn based upon the simulation results. Besides the investigation of some specific PLNs, impact of the physical characteristics of PLC network on the channel delay spread parameters, namely RMS delay spread and maximum excess delay, are studied statistically. Effect of

- number of branching nodes between transmitter and receiver
- separation distance between transmitter and receiver
- length statistics of branches

are analyzed. For each attribute examined, statistics regarding the channel delay spread parameters are presented by observing corresponding cumulative distribution function (CDF) curves. Relations between the attributes listed above and the channel delay parameters are revealed.

This thesis can be considered as a basis for future studies in this field. Future works are planned as

- investigation of noise, multipath, and attenuation characteristics of power line channels for higher frequency ranges up to 100MHz,

- real-time detection of electrical home appliances by investigating the noise they emit into the PLN while they are operating,
- improvement of multipath simulation environment by introducing the AC cycle and frequency dependent impedance values,
- design of a reliable orthogonal frequency division multiplexing (OFDM) based PLC modem.

The purpose of this study is to highlight the importance and the effectiveness of PLC for next generation communication systems.

REFERENCES

[1] S. T. Mak, "A power line communication technology for power distribution network control and monitoring," *Power Delivery, IEEE Transactions on*, vol. 1, no. 1, pp. 66 –72, jan. 1986.

[2] E. Owen, "The origins of 60-hz as a power frequency," *Industry Applications Magazine, IEEE*, vol. 3, no. 6, pp. 8, 10, 12 –14, nov/dec 1997.

[3] Y.-J. Lin, H. Latchman, M. Lee, and S. Katar, "A power line communication network infrastructure for the smart home," *Wireless Communications, IEEE*, vol. 9, no. 6, pp. 104 – 111, dec. 2002.

[4] A. Pasdar and S. Mirzakuchaki, "A solution to remote detecting of illegal electricity usage based on smart metering," aug. 2007, pp. 163 –167.

[5] I. Cavdar, "A solution to remote detection of illegal electricity usage via power line communications," june 2004, pp. 896 – 900 Vol.1.

[6] D. Hong, J. Lee, J. Choi, A. Pasdar, and S. Mirzakuchaki, "Power quality monitoring system using power line communication," Dec. 2005.

[7] D. Cooper and T. Jeans, "Narrowband, low data rate communications on the low-voltage mains in the cenelec frequencies. i. noise and attenuation," *Power Delivery, IEEE Transactions on*, vol. 17, no. 3, pp. 718 – 723, jul 2002.

[8] http://www.homeplug.com, The HomePlug Powerline Alliance.

[9] Y.-J. Lin, H. Latchman, R. Newman, and S. Katar, "A comparative performance study of wireless and power line networks," *Communications Magazine, IEEE*, vol. 41, no. 4, pp. 54 – 63, april 2003.

[10] M. Hazen, "The technology behind homeplug av powerline communications," *Computer*, vol. 41, no. 6, pp. 90 –92, june 2008.

[11] *Draft Standard for Broadband over Power Line Networks: Medium Access Control and Physical Layer Specifications*, http://grouper.ieee.org/groups/1901/index.html, IEEE P1901.

[12] S. Galli and O. Logvinov, "Recent developments in the standardization of power line communications within the ieee," *Communications Magazine, IEEE*, vol. 46, no. 7, pp. 64 –71, july 2008.

[13] H. B. Çelebi, S. Guzelgoz, T. Guzel, H. Arslan, and M. K. Mihcak, "Noise, attenuation and multipath analysis of plc networks," in *2010 European Signal Processing Conference*, Aug 2010, submitted.

[14] S. Guzelgoz, H. B. Çelebi, T. Guzel, H. Arslan, and M. K. Mihcak, "Time frequency analysis of noise generated by electrical loads in plc," in *IEEE International Conference on TElecommunications, ICT*, April 2010, accepted.

[15] S. Guzelgoz, H. B. Çelebi, and H. Arslan, "Articulating factors defining rms delay spread in lv plc channels," *IEEE Transactions on Power Delivery*, submitted.

[16] ——, "Statistical characterization of the paths in multipath plc channels," *IEEE Transactions on Power Delivery*, submitted.

[17] M. Zimmermann, "An analysis of the broadband noise scenario in powerline networks," *Int. Symp. Power-Line Commun. Appl., ISPLC*, 2000.

[18] Balakirsky, "Potential limits on power-line communication over impulsive noise channels," *ISPLC*, 2003.

[19] V. Degardin, M. Lienard, P. Degauque, A. Zeddam, and F. Gauthier, "Impulsive noise on indoor power lines: characterization and mitigation of its effect on plc systems," in *Electromagnetic Compatibility, 2003. EMC '03. 2003 IEEE International Symposium on*, vol. 1, May 2003, pp. 166–169 Vol.1.

[20] D. Umehara, S. Hirata, S. Denno, and Y. Morihiro, "Modeling of impulse noise for indoor broadband power line communications," *Proc. ISITA 2006*, pp. 195–200.

[21] H. Meng, Y. Guan, and S. Chen, "Modeling and analysis of noise effects on broadband power-line communications," *Power Delivery, IEEE Transactions on*, vol. 20, no. 2, pp. 630–637, April 2005.

[22] G. Avril, M. Tlich, F. Moulin, A. Zeddam, and F. Nouvel, "Time/frequency analysis of impulsive noise on powerline channels," *Home Networking*, pp. 143–150.

[23] [Online]. Available: http://www2.ssm.gov.tr/katalog2007/data/397/uruning/19.htm

[24] J. Cortes, F. Canete, L. Diez, and J. Entrambasaguas, "Characterization of the cyclic short-term variation of inddor power-line channel response," in *2005 International Symposium on Power Line Communications and Its Applications.*

[25] F. Corripio, J. Arrabal, L. del Rio, and J. Munoz, "Analysis of the cyclic short-term variation of indoor power line channels," *Selected Areas in Communications, IEEE Journal on*, vol. 24, no. 7, pp. 1327–1338, July 2006.

[26] M. Gotz, M. Rapp, and K. Dostert, "Power line channel characteristics and their effect on communication system design," *Communications Magazine, IEEE*, vol. 42, no. 4, pp. 78 – 86, apr 2004.

[27] H. Meng, Y. Guan, and S. Chen, "Modeling and analysis of noise effects on broadband power-line communications," *ISPLC*, 2002.

[28] N. Andreadou and F.-N. Pavlidou, "Modeling the noise on the ofdm power-line communications system," *Power Delivery, IEEE Transactions on*, vol. 25, no. 1, pp. 150 –157, jan. 2010.

[29] R. Hormis, I. Berenguer, and X. Wang, "A simple baseband transmission scheme for power line channels," *Selected Areas in Communications, IEEE Journal on*, vol. 24, no. 7, pp. 1351 – 1363, july 2006.

[30] W. Bo, Q. Yinghao, H. Peiwei, and C. Wenhao, "Indoor powerline channel simulation and capacity analysis," dec. 2007, pp. 154 –157.

[31] M. Zimmermann and K. Dostert, "Analysis and modeling of impulsive noise in broadband powerline communications," *Electromagnetic Compatibility, IEEE Transactions on*, vol. 44, no. 1, pp. 249 –258, feb 2002.

[32] V. Degardin, M. Lienard, A. Zeddam, F. Gauthier, and P. Degauquel, "Classification and characterization of impulsive noise on indoor powerline used for data communications," *Consumer Electronics, IEEE Transactions on*, vol. 48, no. 4, pp. 913 – 918, nov 2002.

[33] M. Zimmermann and K. Dostert, "A multipath model for the powerline channel," *Communications, IEEE Transactions on*, vol. 50, no. 4, pp. 553–559, Apr 2002.

[34] ——, "A multi-path signal propagation model for the power line channel in the high frequency range," *Int. Symp. Power-Line Commun. Appl., ISPLC*, 1999.

[35] T. S. Rappaport, *Microwave Engineering*. Toronto: John Wiley & Sons, 1998.

[36] R. A. Chipman, *Schaum's Outline of Theory and Problems of Transmission Lines*. New York: McGrow-Hill, 1968.

[37] T. Maenou and M. Katayama, "Study on signal attenuation characteristics in power line communications," 0-0 2006, pp. 217 –221.

[38] H. Phillips, "Modeling of powerline communication channels," in *Proceedings of International Symposium on Power LineCommunications and Its Applications*, 1999.

[39] C. Hensen and W. Schulz, "Time dependence of the channel characteristics of low voltage power-lines and its effects on hardware implementation," in *AEU Int'l. J. Electronics and Commun.*, vol. 54, no. 1, Feb 2000, pp. 23–32.

[40] D. Anastasiadou and T. Antonakopoulos, "Multipath characterization of indoor powerline networks," *Power Delivery, IEEE Transactions on*, vol. 20, no. 1, pp. 90–99, Jan. 2005.

[41] T. Banwell and S. Galli, "A novel approach to the modeling of the indoor power line channel part i: circuit analysis and companion model," *Power Delivery, IEEE Transactions on*, vol. 20, no. 2, pp. 655–663, April 2005.

[42] ——, "A novel approach to the modeling of the indoor power line channel part 2: Transfer functions and its properties," *Power Delivery, IEEE Transactions on*, vol. 20, no. 3, pp. 1869–1878, July 2005.

[43] T. Rappaport, *Wireless communications: principles and practice*. Prentice Hall PTR Upper Saddle River, NJ, USA, 2001.

[44] J. Anatory, N. Theethayi, R. Thottappillil, and N. Mvungi, "A broadband power-line communication system design scheme for typical tanzanian low-voltage network," *Power Delivery, IEEE Transactions on*, vol. 24, no. 3, pp. 1218 –1224, july 2009.

[45] J. Anatory, N. Theethayi, and R. Thottappillil, "Channel characterization for indoor power-line networks," *Power Delivery, IEEE Transactions on*, vol. 24, no. 4, pp. 1883 –1888, oct. 2009.

[46] ——, "Performance of underground cables that use ofdm systems for broadband power-line communications," *Power Delivery, IEEE Transactions on*, vol. 24, no. 4, pp. 1889 –1897, oct. 2009.

[47] J. Anatory, N. Theethayi, R. Thottappillil, M. Kissaka, and N. Mvungi, "The influence of load impedance, line length, and branches on underground cable power-line communications (plc) systems," *Power Delivery, IEEE Transactions on*, vol. 23, no. 1, pp. 180 –187, jan. 2008.

[48] ——, "Broadband power-line communications: The channel capacity analysis," *Power Delivery, IEEE Transactions on*, vol. 23, no. 1, pp. 164 –170, jan. 2008.

[49] J. Anatory, M. M. Kissaka, and N. H. Mvungi, "Channel model for broadband power-line communication," *Power Delivery, IEEE Transactions on*, vol. 22, no. 1, pp. 135 –141, jan. 2007.

[50] J. Anatory, N. Theethayi, R. Thottappillil, M. Kissaka, and N. Mvungi, "The effects of load impedance, line length, and branches in the bplc; transmission-line analysis for indoor voltage channel," *Power Delivery, IEEE Transactions on*, vol. 22, no. 4, pp. 2150 –2155, oct. 2007.

[51] C. Konate, M. Machmoum, and J. Diouris, "Multi path model for power line communication channel in the frequency range of 1mhz-30mhz," sept. 2007, pp. 984 –989.

[52] H. Meng, S. Chen, Y. Guan, C. Law, P. So, E. Gunawan, and T. Lie, "Modeling of transfer characteristics for the broadband power line communication channel," *Power Delivery, IEEE Transactions on*, vol. 19, no. 3, pp. 1057 – 1064, july 2004.

[53] Y. T. Ma, K. H. Liu, and Y. N. Guo, "Artificial neural network modeling approach to power-line communication multi-path channel," june 2008, pp. 229 –232.

[54] I. Papaleonidopoulos, C. Capsalis, C. Karagiannopoulos, and N. Theodorou, "Statistical analysis and simulation of indoor single-phase low voltage power-line communication channels on the basis of multipath propagation," *Consumer Electronics, IEEE Transactions on*, vol. 49, no. 1, feb. 2003.

APPENDICES

Appendix A Calculation of Reflection and Transmission Coefficients

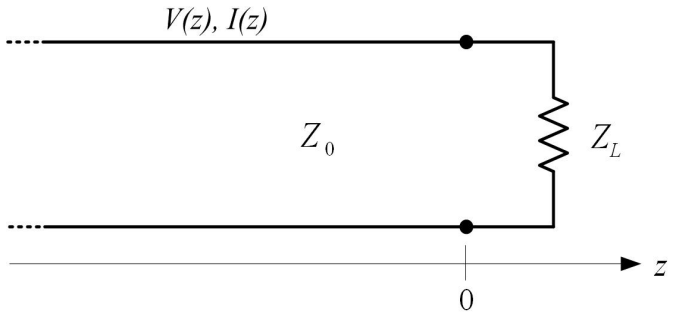

Figure A.1 Terminated lossless transmission line

Reflection coefficient in transmission lines is analyzed in a terminated lossless transmission line as depicted in Fig. A.1.

The total voltage on line can be written as the sum of the incident and reflected waves

$$V(z) = V_0^+ e^{-j\beta z} + V_0^- e^{j\beta z} \tag{A.1}$$

$$I(z) = \frac{V_0^+}{Z_0} e^{-j\beta z} + \frac{V_0^-}{Z_0} e^{j\beta z} \tag{A.2}$$

where V_0^+ is the amplitude of incident wave and $e^{j\cdots}$ shows the phase difference. The total voltage and current at the load are related by the load impedance, so at $z = 0$

$$Z_L = \frac{V_0^+ e^{-j\beta z} + V_0^- e^{j\beta z}}{\frac{V_0^+}{Z_0} e^{-j\beta z} + \frac{V_0^-}{Z_0} e^{j\beta z}} \tag{A.3}$$

$$Z_L = \frac{V(0)}{I(0)} = \frac{V_0^+ + V_0^-}{I_0^+ - I_0^-} Z_0 \qquad \text{where} \quad z = 0 \tag{A.4}$$

Since the reflection coefficient is the ratio between the incident and reflected waves, reflection coefficient can be written as

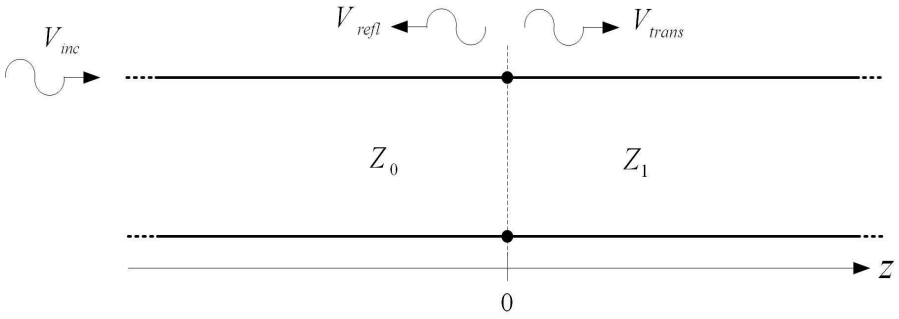

Figure A.2 Transmission line feeding a line of different characteristic impedance

$$\Gamma = \frac{V_0^-}{V_0^+} \tag{A.5}$$

where Γ represents the reflection coefficient. If we solve (A.4) for V_0^-

$$V_0^- = \frac{Z_L - Z_0}{Z_L + Z_0} V_0^+ \tag{A.6}$$

So the term reflection coefficient can be written as

$$\Gamma = \frac{Z_L - Z_0}{Z_L + Z_0} \tag{A.7}$$

Transmission coefficient describes the amplitude of the transmitted wave relative to the incident wave. In order to derive the transmission coefficient, consider a transmission line connected to another line of different characteristic impedance. If the load line is infinitely long and terminated with its own characteristic impedance, it can be assumed that no reflections will receive from its end. A transmission line feeding another one is depicted in Fig. A.2.

Appendix A (Continued)

If the transmission coefficient is shown with T

$$V_{refl} = \Gamma V_0^+ \quad \text{where} \quad \Gamma = \frac{Z_1 - Z_0}{Z_1 + Z_0} \tag{A.8}$$

$$V_{trans} = T V_0^+ \tag{A.9}$$

So the voltage for $z < 0$ and for $z > 0$, in the absence of reflections, can be written as

$$V(z) = V_0^+ e^{-j\beta z}(1 + \Gamma e^{j2\beta z}) \quad \text{for} \quad z < 0 \tag{A.10}$$

$$V(z) = T V_0^+ e^{-j\beta z} \quad \text{for} \quad z > 0 \tag{A.11}$$

The total voltage at $z = 0$ should be equal. By equating (A.10) and (A.11) at $z = 0$

$$V_0^+ e^{-j\beta z}(1 + \Gamma e^{j2\beta z}) = T V_0^+ e^{-j\beta z} \quad \text{for} \quad z = 0 \tag{A.12}$$

by solving (A.12) transmission coefficient can be calculated as

$$T = 1 + \Gamma \tag{A.13}$$

$$T = 1 + \frac{Z_1 - Z_0}{Z_1 + Z_0} \tag{A.14}$$

$$T = \frac{2Z_1}{Z_1 + Z_0} \tag{A.15}$$

It is obvious that reflection coefficient can get a value between $[-1, 1]$, where reflection coefficient of -1 represents the termination ended by short circuit and 1 represents a termination ended with open circuit. Consequently, it may be surprising but T may be greater

than unity. However, it should be kept in mind that Γ and T are the relative values of the voltage of the signal. While extracting these coefficients, current values did not analyzed.

In order to show the accuracy of this statement, power values of the incident wave and reflected and transmitted waves are compared. According to the conservation of energy, the total power of the signals after the impedance discontinuity point should remain same with the power of the incident signal.

If the transmission line depicted in Fig.A.2 is taken into consideration, voltage and current values on the line for $z < 0$ are

$$V_{z<0}(z) = V_0^+ e^{-j\beta z}(1 + \Gamma e^{2j\beta z}) \tag{A.16}$$

$$I_{z<0}(z) = \frac{V_0^+}{Z_0} e^{-j\beta z}(1 - \Gamma e^{2j\beta z}) \tag{A.17}$$

The time-average power flow along the line for $z < 0$ is

$$P_{z<0} = \frac{1}{2}\mathrm{Re}\big[V_{z<0}(z) \cdot I_{z<0}(z)^*\big] \tag{A.18}$$

$$= \frac{1}{2}\mathrm{Re}\big[V_0^+ e^{-j\beta z}(1 + \Gamma e^{2j\beta z}) \frac{\left(V_0^+\right)^*}{Z_0} e^{j\beta z}(1 - \Gamma^* e^{-2j\beta z})\big] \tag{A.19}$$

$$= \frac{\left|V_0^+\right|^2}{2Z_0}\mathrm{Re}\big[1 - \Gamma^* e^{-2j\beta z} + \Gamma e^{2j\beta z} - |\Gamma|^2\big] \tag{A.20}$$

Please note that, characteristic impedance values are mostly real numbers as explained in Sec. 4.2.1. The middle two terms in the brackets are of the term form $x - x^* = 2j\mathrm{Im}(x)$ and so they are purely imaginary. This simplifies the result to

Appendix A (Continued)

$$P_{z<0} = \frac{\left|V_0^+\right|^2}{2Z_0}(1-|\Gamma|^2) \tag{A.21}$$

$$= \underbrace{\frac{\left|V_0^+\right|^2}{2Z_0}}_{P_{inc}} - \underbrace{|\Gamma|^2\frac{\left|V_0^+\right|^2}{2Z_0}}_{P_{refl}} \tag{A.22}$$

The time-average power flow along the line for $z > 0$, which is equal to the power of transmitted wave, is

$$P_{z>0} = \frac{1}{2}\mathrm{Re}\big[V_{z>0}(z)\cdot I_{z>0}(z)^*\big] \tag{A.23}$$

where

$$V_{z>0}(z) = TV_0^+e^{-j\beta z} \tag{A.24}$$

$$I_{z>0}(z) = T\frac{V_0^+}{Z_1}e^{-j\beta z} \quad \text{for} \quad z>0 \tag{A.25}$$

then

$$P_{z>0} = \frac{1}{2}\mathrm{Re}\big[TV_0^+e^{-j\beta z}T^*\frac{\left(V_0^+\right)^*}{Z_1}e^{j\beta z}\big] \tag{A.26}$$

$$= \frac{\left|T\right|^2\left|V_0^+\right|^2}{2Z_1} \tag{A.27}$$

According to the conservation of energy

$$P_{inc} = P_{refl} + P_{trans} \tag{A.28}$$

equality should be maintained. Power of the incident wave is

$$P_{inc} = \frac{\left|V_0^+\right|^2}{2Z_0} \tag{A.29}$$

and the total power of reflected and transmitted waves can be written as

$$P_{refl} + P_{trans} = \frac{\left|\Gamma\right|^2\left|V_0^+\right|^2}{2Z_0} + \frac{\left|T\right|^2\left|V_0^+\right|^2}{2Z_1} \tag{A.30}$$

$$= \frac{\left|V_0^+\right|^2}{2}\Big(\frac{\left|\Gamma\right|^2}{Z_0} + \frac{\left|T\right|^2}{Z_1}\Big) \tag{A.31}$$

$$= \frac{\left|V_0^+\right|^2}{2}\Big(\frac{Z_0^2 + Z_1^2 - 2Z_1Z_0}{Z_0(Z_0+Z_1)^2} + \frac{4Z_1^2}{Z_1(Z_0^2+Z_1^2)}\Big) \tag{A.32}$$

$$= \frac{\left|V_0^+\right|^2}{2}\frac{(Z_0+Z_1)^2}{Z_0(Z_0+Z_1)^2} \tag{A.33}$$

$$= \frac{\left|V_0^+\right|^2}{2Z_0} \tag{A.34}$$

so

$$P_{inc} = P_{refl} + P_{trans} \quad \text{is achieved for} \quad T = 1 + \Gamma \tag{A.35}$$

which proves that, it is possible to find values of transmission coefficient that are greater than unity.